https://doi.org/10.5194/egusphere-2024-2709
Preprint. Discussion started: 7 October 2024
© Author(s) 2024. CC BY 4.0 License.

Spatio-temporal variations in surface Marine Carbonate System properties across the Western Mediterranean Sea using Volunteer Observing Ship data.

David Curbelo-Hernández*, David González-Santana, Aridane González-González, J. Magdalena Santana-Casiano and Melchor González-Dávila

[1] Instituto de Oceanografía y Cambio Global (IOCAG), Universidad de Las Palmas de Gran Canaria (ULPGC). Las Palmas de Gran Canaria, Spain.

* Corresponding Author: david.curbelo@ulpgc.es

https://doi.org/10.5194/egusphere-2024-2709
Preprint. Discussion started: 7 October 2024
© Author(s) 2024. CC BY 4.0 License.

Abstract

The surface physical and Marine Carbonate System (MCS) properties were assessed along the western boundary of the Mediterranean Sea. An unprecedent high-resolution observation-based dataset spanning 5 years (2019-2024) was built through automatically underway monitoring by a Volunteer Observing Ship (VOS). The MCS dynamics were strongly modulated by physical-biological coupling dependent on the upper-layer circulation and mesoscale features. On a seasonal scale, the variations in CO_2 fugacity ($fCO_{2,sw}$) were mainly driven by sea surface temperature (SST) fluctuations (45-83%) and partially offset by the processes controlling total inorganic carbon (C_T) distribution (25-38%). On an interannual scale, the SST trends (0.26-0.43 ºC yr^{-1}) have accelerated by 78-88% in comparison with previous decades. The ongoing surface warming was the main factor (with a contribution of ~76-92%) increasing $fCO_{2,sw}$ (4.18 to 5.53 µatm yr^{-1}) and, consequently, decreasing pH (-0.005 to -0.007 units yr^{-1}) in the surface waters. The seasonal SST, becoming larger due to progressively warmer summers, was the primary driver of the observed slope up of interannual trends. The evaluation of the air-sea CO_2 exchange shows the area across the Alboran Sea (14,000 Km^2) and the eastern Iberian margin (40,000 Km^2) acting as an atmospheric CO_2 sink of -1.57 ± 0.49 mol m^{-2} yr^{-1} (0.97 ± 0.30 Tg CO_2 yr^{-1}) and -0.70 ± 0.54 mol m^{-2} yr^{-1} (-1.22 ± 0.95 Tg CO_2 yr^{-1}), respectively. The net annual CO_2 sink has reduced by 40-80% since 2019 due to the ongoing strength of the source status during summer and the weakening in the sink status during spring and autumn.

Keywords: Marine Carbonate System, Air-sea CO_2 fluxes, Volunteer Observing Ships, Western Mediterranean Sea, ocean acidification, sea-surface warming

https://doi.org/10.5194/egusphere-2024-2709
Preprint. Discussion started: 7 October 2024
© Author(s) 2024. CC BY 4.0 License.

1. Introduction

The semi-enclosed and marginal seas have a relevant role in the global biogeochemical cycles and are highly vulnerable to climate change (IPCC, 2023). These regions accomplish extensive coastal and continental shelf and slope areas occupied with multiple diverse ecosystems under anthropogenic pressure. Although these regions present enhanced biogeochemical activity and intensified air-sea CO_2 exchange rates compared to the open ocean (Borges et al., 2005; Cai et al., 2006; Frankignoulle and Borges, 2001; Shadwick et al., 2010), its poorly monitoring and assessment have historically excluded them from global studies and models and underestimated in the Global Carbon Budget (Friedlingstein et al., 2023)

The Mediterranean Sea is a dynamic semi-enclosed system potentially fragile to natural and anthropogenic forcing (e. g. Álvarez et al., 2014; Tanhua et al., 2013). The particular oceanography of the Mediterranean Sea, collectively described in several works (e.g. Nielsen, 1912; Robinson et al., 2001; Millot and Taupier-Letage, 2005; Bergamasco and Malanotte-Rizzoli, 2010; Schroeder et al., 2012), have rendered it a "miniature ocean" considered as "laboratory basin" to evaluate physico-chemical perturbations that can be extrapolated to larger scales in the global ocean (e.g. Robinson and Golnaraghi, 1994; Bergamasco and Malanotte-Rizzoli, 2010). These perturbations have accelerated since the second half of the 20^{th} century, with temperature and salinity increasing at unprecedent rates of 0.04ºC and 0.015 per decade, respectively (Borghini et al., 2014), impacting the Marine Carbonate System (MCS). However, the availability of high-quality observation-based data and research in this basin is scarce due to spatial and temporal limitations in the monitoring and sampling techniques (Millero et al., 1979; Rivaro et al., 2010).

The MCS dynamics has been evaluated in the Northwestern Mediterranean basin (Bégovic and Copin-Montégut, 2002; Copin-Montégut and Bégovic, 2002, 2004; Coppola et al., 2020; Hood and Merlivat, 2001; Mémery et al., 2002; Merlivat et al., 2018; Touratier and Goyet, 2009; Ulses et al., 2023), mainly conducted at the time-series DYFAMED (43.42 ºN, 7.87 ºE; Marty, 2002) and BOUSSOLE sites (43.37° N, 7.90° E; Antoine et al., 2006, 2008a, 2008b). These investigations have shown the seasonal cycle of the surface CO_2 is primarily governed by thermal fluctuations and the behaviour of the area as a relatively weak sink for atmospheric CO_2 on an annual scale. Long-term changes

https://doi.org/10.5194/egusphere-2024-2709
Preprint. Discussion started: 7 October 2024
© Author(s) 2024. CC BY 4.0 License.

estimated by Merlivat et al., (2018) reported the increase in the surface CO_2 fugacity ($fCO_{2,sw}$) and pH of ~40 µatm and ~0.04 units, respectively, since the 90s. The interannual trends given for $fCO_{2,sw}$ (2.3 ± 0.23 µatm yr^{-1}; Merlivat et al., 2018) and pH (0.002-0.003 units yr^{-1}; Yao et al., 2016) were in agreement with those encountered in the Northeast Atlantic at the ESTOC site (2.1 ± 0.1 µatm yr^{-1} and 0.002 ± 0.0001 units yr^{-1}, respectively; González-Dávila and Santana-Casiano, 2023). Although the Northwestern Mediterranean is characterized by a relatively strong atmospheric CO_2 uptake and storage due to deep-convection (Copin-Montégut, 1993; D'Ortenzio et al., 2008; Cossarini et al., 2021), the long-term variations in MCS occur at rates larger than the expected from the chemical equilibrium with the atmospheric CO_2. It has been attributed to the substantial input of anthropogenic carbon from the North Atlantic (Merlivat et al., 2018; Palmiéri et al., 2015; Schneider et al., 2010; Ulses et al., 2023). Based on a high-resolution regional model, Palmiéri et al., (2015) estimated that ~25% of the anthropogenic carbon storage in the Mediterranean Sea comes from the Atlantic. The water exchange processes in the Strait of Gibraltar become the western boundary of the Mediterranean Sea in a crucial region for MCS variability which significantly modulates the basin-wide anthropogenic carbon inventory and ocean acidification trends in the Mediterranean basin and could affect significantly the general circulation and the composition of seawaters in the North Atlantic. Additionally, this region is subject to variability related with (1) the intense deep-water convection in the adjacent Northwestern area of the Mediterranean Sea and (2) the unique circulation patterns shaped to the irregular coastlines and islands, which forms quasi-permanent eddies and other (sub)mesoscale features (Alberola et al., 1995; Bosse et al., 2021; 2016; Bourg and Molcard, 2021).

The Western Mediterranean Sea encompasses the Alboran Sea, land-loaded by the southern Iberian Peninsula coast and northern African coast, and the coastal transitional area along the eastern Iberian margin (Figure 1a). The classical surface circulation pattern in the Alboran Sea (e. g. Bormans and Garrett, 1989; Peliz et al., 2013; Sánchez-Garrido et al., 2013, 2022; Speich, 1996; Whitehead and Miller, 1979), with the Atlantic water jet (AJ) following wavelike path of the quasi-permanent Western Anticyclonic Gyre (WAG) and the Eastern Anticyclonic Gyre (EAG) and constituting the Modified Atlantic Water (MAW; Lopez-García et al., 1994; Viúdez et al., 1998), drive west-to-east variations in physical and biogeochemical terms. The intensity and direction of the AJ, depending primarily on sea level pressure and local wind fluctuations, variate on different timescales

https://doi.org/10.5194/egusphere-2024-2709
Preprint. Discussion started: 7 October 2024
© Author(s) 2024. CC BY 4.0 License.

and govern the circulation patterns in the Alboran Sea influencing the biogeochemistry (Sánchez-Garrido and Nadal, 2022; Solé et al., 2016). On a seasonal scale, the AJ oscillate between two main circulation modes (García-Lafuente et al., 2002; Macías et al., 2008, 2016; Vargas-Yáez et al., 2002), detectable by reanalysis data-based SST signals (Figure 1b): a high-intense AJ flowing north-eastward during spring/summer and a lower-intense AJ flowing with more south-eastwardly direction during autumn/winter. The stronger AJ during the warm months feed the classical two-gyres configuration in the Alboran Sea, while the weak AJ only allows the exitance of the WAG (Renault et al., 2012). The AJ forms a filament flowing from the Iberian coastal upwelling in the northwestern Alboran Sea and surrounding the eastern edge of the WAG, which is most frequently presented during summer (Gómez-jakobsen et al., 2019; Millot, 1999). The westernmost part of the Alboran Sea is affected by the shallow position of the Atlantic-Meridional Interface layer (AMI; Bray et al., 1995; Lacombe and Richez, 1982), which promotes the injection of deep-water into the surface (Echevarría et al., 2002; Gómez-jakobsen et al., 2019; Minas et al., 1991).

The eastern Iberian margin is influenced by the path of the Northern Current transporting Mediterranean Water (MW; Pinot et al., 1995), which is originated around the Gulf of Lion where the forcing of the northeasterly winds is frequently strong and flows southward along the eastern coastline of the Iberian Peninsula (Conan and Millot, 1995; Millot, 1999; Sammari et al., 1995). The seasonality of the Northern Current (Millot, 1999) infers meridional variations in the thermal signals between cold and warm months (Figure 1b). The enhanced wind-forcing during winter intensify the Northern Current, which fit to the Iberian continental slope and recirculate offshore at Cape of Nao, while a low-intense branch progress southward Cape of Nao and reach the eastern Alboran Sea. The weakening in the wind-forcing forms a surface thermal front in the axis of the Pyrenees during summer and changed the path of the Northern Current further away from the Iberian coast (Lopez-García et al., 1994), which allow the MAW to reach its northern most spreading.

This research focus on the surface spatio-temporal variations of the MCS and air-sea CO_2 fluxes in the western boundary of the Mediterranean Sea. An alternatively and efficiently observation-based method that ensures high-frequency and quality data was used: the autonomous underway monitoring of the surface ocean by a Volunteer Observing ship

https://doi.org/10.5194/egusphere-2024-2709
Preprint. Discussion started: 7 October 2024
© Author(s) 2024. CC BY 4.0 License.

(VOS). This systematic strategy represents a powerful tool to analyse the distribution and changes of physical and MCS properties in highly variable areas as coastal transitional zones where the availability of data has been historically scarce. The dataset used was built based on continuous observations along the SOOP CanOA-VOS line (Curbelo-Hernández et al., 2021a; 2021b) from February 2019 to February 2024. The cruise track (Figure 1) followed the south and east geographically rugged coastline of the Iberian Peninsula and allowed the characterization of the Alboran Sea (~2-5.1ºW) separately from the eastern coastal and shelf area between Cape of Gata (Almería) and Barcelona (~36.5-41.3ºN). The changes observed in the MCS on a seasonal and interannual timescales (even considering the limitations of 5 years of data), the mechanism controlling their variations and the changes in the air-sea CO_2 exchange have been attended in this study, contributing to improve our knowledge in a key oceanographic region.

2. Material and methods

2.1.Data collection

A high spatio-temporal resolution dataset spanning 5 years was constructed based on weekly physico-chemical observations of the surface western boundary of the Mediterranean Sea between February 2019 and February 2024. Data was automatically collected by a Surface Ocean Observation Platform (SOOP) running in underway mode and placed aboard the Volunteer Observing Ship (VOS) MV JONA SOPHIE (IMO: 9144718, called RENATE P before November 2021), a container ship managed in Spain by Nisa Maritima which links the Canary Islands with Barcelona.

The SOOP CanOA-VOS line allows the monitoring of the northeast archipelagic waters of the Canary Islands and coastal transitional waters of the Northeast Atlantic (Curbelo-Hernández et al., 2021), the Strait of Gibraltar (Curbelo-Hernández et al., 2021) and the western Mediterranean Sea (Figure 1). The system operates fully unattended with biweekly (time required to complete a round trip) routine maintenance at the port of Las Palmas de Gran Canaria (28.13 ºN, 15.42 ºW). The automatic transfer of data to a server occurs each time the vessel docks at each of the port along the usual route (Las Palmas de Gran Canaria, Santa Cruz de Tenerife, Arrecife, Sagunto and Barcelona). A total of 92 routes were completed in the Mediterranean Sea (Figure 1).

The SOOP CanOA-VOS line, which was designed and is maintained by the QUIMA research group at the IOCAG-ULPGC, is part of the Spanish contribution to the Integrated Carbon Observation System (ICOS-ERIC; https://www.icos-cp.eu/) since 2021 and has been recognized as an ICOS Class 1 Ocean Station. Therefore, the measurement equipment and underway data collection techniques verify the ICOS-ERIC high-quality requirements and methodological recommendations.

2.2. Monitoring routines

The autonomous underway monitoring of CO_2 in surface ocean and low atmosphere and the data collection routines followed the recommendations described by Pierrot et al., (2009) to ensure comparable and high-quality datasets. An automated underway CO_2 molar fraction (xCO_2, ppm) measurement system, developed by Craig Nail and commercialized by General Oceanics™, was installed inside the engine room of the SOOP CanOA-VOS and described in detail by Curbelo et al. (2021a, 2021b).

The xCO_2 measurement system combines an air and seawater equilibrator, placed inside the wet box, with a non-dispersive infrared analyser for gas detection, placed inside the dry box. The analyser used for xCO_2 detection was built by LICOR® (initially the 6262 model and after October 2019, a 7000 model). The analyser is automatically calibrated on departure and arrival at each port and periodically in loop every three hours using four standard gases. Additionally, the system is zeroed and spanned (with standard gases 1 and 4, respectively) every twelve hours to properly interpolate the standard values and correct for instrument drift. The four standard gases, with an accuracy of ±0.02 ppm, were provided by the National Ocean and Atmospheric Administration (NOAA) and traceable to the World Meteorological Organization (WMO). They were in the order of 0 ppm, 250 ppm, 400 ppm and 550 ppm until January 2021, when the gas bottles for standard 2 to 4 were changed for a new set with concentrations in the order of 300 ppm, 500 ppm and 800 ppm provided by the ICOS central analytical laboratories.

The sea surface temperature (SST, in ºC) was monitored by using a SBE38 thermometer placed at the primary seawater intake in the engine room, with a reported error of ±0.01ºC. The high sensitivity of xCO_2 to temperature fluctuations required to measure the temperature at different locations along the system. A SBE45 thermosalinograph and a Hart Scientific HT1523 Handheld Thermometer, with reported errors of ±0.01ºC, were used to monitor the temperature at the entrance of the wet box and inside the equilibrator,

https://doi.org/10.5194/egusphere-2024-2709
Preprint. Discussion started: 7 October 2024
© Author(s) 2024. CC BY 4.0 License.

respectively. The SBE45 thermosalinograph measured the sea surface salinity (SSS) with an estimated error of ±0.005. Lastly, the atmospheric pressure is monitored at the deck box transducer, while the differential pressure with the ambient air is also controlled in the wet box inside the equilibrator and in the dry box inside the analyser. The atmospheric pressure records can differ in the order of milibars with the pressure inside the engine room due to the forcing of ventilation.

Discrete surface seawater samples were manually collected with in situ records of SST and SSS during three round trips in February 2020, March 2021 and October 2023. The discrete sampling was performed along the vessel track from the seawater supply line every 1-2 hours in borosilicate glass bottles, overfilled and preserved with 100 µl of saturated $HgCl_2$. Samples were kept in dark and analysed just after arriving at port, in a period less than 2 weeks, for total alkalinity (A_T, µmol kg^{-1}) and total dissolved inorganic carbon (C_T, µmol kg^{-1}) determination A total of 102 discrete samples has been collected in the Mediterranean Sea.

The underway observational dataset exhibits a gap of a year among September 2021 and 2022 due to the temporary cessation of the measurement system for vessel maintenance activities in dry dock. During this period, the measurement system was sent for calibration and maintenance to General Oceanics enterprise, Miami, USA. There are also several gaps of less than a month related with different technical issues with the measurement equipment, which were addressed during the routine maintenance visits to the vessel (i. e. problems with the pump and seawater intake, with the LICOR analyser, depletion of gas bottles supplies, electrical issues in the engine room). Certain technical issues encountered during 2020 were delayed in being resolved due to the constraints imposed by COVID-19.

2.3. Calculation procedures

2.3.1. CO_2 system variables

The present investigation followed the data collection methodology, quality control and calculation procedures as published in the updated version of the DOE method manual for ocean CO_2 analysis (Dickson et al., 2007). The post-cruises correction of the measured xCO_2 and calculation of the fugacity of CO_2 in surface seawater ($fCO_{2,sw}$) and in the lower atmosphere ($fCO_{2,atm}$) followed the procedure described by Pierrot et al. (2009). The full set of standard gases was linearly interpolated to the time of observations to generate the calibration curve used for xCO_2 correction before calculating fCO_2.

The discrete seawater samples were analysed for A_T and C_T by using a VINDTA 3C and following the procedure detailed by Mintrop et al., (2000).. The VINDTA 3C was calibrated through the titration of Certified Reference Material (CRMs; provided by A. Dickson at Scripps Institution of Oceanography), giving values with an accuracy of ±1.5 μmol kg^{-1} for A_T and ±1.0 μmol kg^{-1} for C_T. The A_T was calculated at the times of the observations as previously done in the Northeast Atlantic (Curbelo-Hernández et al., 2021; 2023) and in the Strait of Gibraltar (Curbelo-Hernández et al., 2021), using the A_T-SSS linear relationship obtained from the discrete samples (Eq. 1), which is statistically significant at the 99% level of confidence (p-value < 0.01; r^2= 0.92). The change in A_T with SSS was assumed as constant through the entire annual cycle at this latitudes (Lee et al., 2006). The A_T-SSS relationship provided here can be used to calculate the A_T content of surface seawaters in the Mediterranean Sea with salinities ranging between 36 and 38.5 and with a standard error of estimate of ±17.1 μmol kg^{-1} (<0.7%).

$$A_T = 101.4\ (\pm 6.3)\ SSS - 1303\ (\pm 234) \quad (1)$$

The pH and C_T were calculated at the times of the underway observations by using the CO_{2SYS} programme developed by Lewis and Wallace, (1998) and run with the MATLAB software (van Heuven et al., 2011; Orr et al., 2018; Sharp et al., 2023). The $fCO_{2,sw}$ and A_T were used as input CO_2 system variables. The set of constant used for computations includes the carbonic acid dissociation constants of Lueker et al., (2000), the HSO_4 dissociation constant of Dickson, (1990), the HF dissociation constant of Perez and Fraga, (1987) and the value of $[B]_T$ determined by Lee et al., (2010). The effect of temperature on pH was removed by computation at a constant temperature of 19ºC, which is the mean temperature within the observational period (referred as pH_{19}).

2.3.2. Thermal and non-thermal $fCO_{2,sw}$

The contribution of the thermal and non-thermal processes on the variation of $fCO_{2,sw}$ has been addressed. The non-thermal processes mainly include the biological and carbonate pumps, circulation patterns and air-sea gas exchange (De Carlo et al., 2013). The collectively known methodology presented by Takahashi et al., (2002) with the

© Author(s) 2024. CC BY 4.0 License.

experimentally-determined temperature effects on pCO_2 for isochemical seawater of 0.0423 ºC^{-1} (Takahashi et al., 1993) was used. This procedure has been previously applied to SOOP CanOA-VOS data and detailed by Curbelo-Hernández et al., (2021a; 2021b). An alternative procedure recently introduced by Fassbender et al., (2022) and detailed by Rodgers et al., (2023),modified from the Takahashi et al., (2002, 1993) framework was also used in this investigation. This updated method addresses the slightly variations in the thermal sensitivity of $fCO_{2,sw}$ due to background chemistry (Wanninkhof et al., 1999, 2022), which introduces slightly difference between the observed seasonal cycle of $fCO_{2,sw}$ and the calculated through the sum of its thermal and non-thermal components.

The new approach for the thermal component of $fCO_{2,sw}$ ($fCO_{2,\ T\ FASS}$) was computed from the annual means (denoted with the subscripts AM) of SSS, A_T and C_T at in situ temperature (Eq. 2) by using the CO_{2SYS} programme (Lewis and Wallace, 1998) for MATLAB (van Heuven et al., 2011; Orr et al., 2018; Sharp et al., 2023).

$$fCO_{2,\ T\ FASS} = CO_{2,SYS}(C_{T,AM}, A_{T,AM}, SSS_{AM}, SST) \quad (2)$$

The thermal-driven change in $fCO_{2,sw}$ ($fCO_{2,\ T\ anom}$) can be calculated as the difference between the thermal component of $fCO_{2,sw}$ ($fCO_{2,\ T\ FASS}$) and the annual mean of $fCO_{2,sw}$ (Eq. 3). The non-thermal component ($fCO_{2,\ NT\ FASS}$) is given by the difference between the $fCO_{2,sw}$ at the times of observations and the $fCO_{2,\ T\ anom}$ (Eq. 4). The difference among $fCO_{2,\ NT\ FASS}$ and the annual mean of $fCO_{2,sw}$ provides the change in $fCO_{2,sw}$ explained by non-thermal processes ($fCO_{2,\ NT\ anom}$) (Eq. 5).

$$fCO_{2,\ T\ anom} = fCO_{2,\ T\ FASS} - fCO_{2,\ AM} \quad (3)$$

$$fCO_{2,\ NT\ FASS} = fCO_{2,sw} - fCO_{2,\ T\ anom} \quad (4)$$

$$fCO_{2,\ NT\ anom} = fCO_{2,\ NT\ FASS} - fCO_{2,\ AM} \quad (5)$$

The relative importance of thermal and non-thermal processes was expressed by the T/B ratio ($\Delta fCO_{2,thermal}/\Delta fCO_{2,non-thermal}$), with values greater than 1 indicating that the temperature effect govern the $fCO_{2,sw}$ variations.

2.3.3. Factors controlling the seasonality of $fCO_{2,sw}$

https://doi.org/10.5194/egusphere-2024-2709
Preprint. Discussion started: 7 October 2024
© Author(s) 2024. CC BY 4.0 License.

The changes in the surface $fCO_{2,sw}$ result from the combined variation in the physical and biochemical seawater properties. The seasonal variability of the surface $fCO_{2,sw}$ was addressed by attending the partial contribution of SST, SSS, C_T and A_T. The influence of each driver was quantified by assuming linearity and employing a first-order Taylor-series deconvolution (Sarmiento and Gruber, 2006) given in Eq. 6 and previously used for pCO_2 (Doney et al., 2009; Lovenduski et al., 2007; Takahashi et al., 1993; Turi et al., 2014) and pH (Fröb et al., 2019; García-Ibáñez et al., 2016; Pérez et al., 2021; Takahashi et al., 1993; Curbelo-Hernández et al., 2024). Due to the high relevance of the evaporation/precipitation processes in the Mediterranean Sea and in order to avoid the influence of river discharge and other freshwater fluxes along the south and east coast of the Iberian Peninsula, the most recent equation (Eq. 7) given by Pérez et al., (2021) with salinity-normalized C_T and A_T ($NX_T = X_T/S*37.4$) was used. The C_T and A_T were normalized (NC_T and NA_T) to a constant salinity of 37.4, the average for the entire monitored area ($NX_T = X_T/SSS*37.4$).

$$\frac{dpCO_2}{dt} = \frac{\partial pCO_2}{\partial SST}\frac{dSST}{dt} + \frac{\partial pCO_2}{\partial SSS}\frac{dSSS}{dt} + \frac{\partial pCO_2}{\partial C_T}\frac{dC_T}{dt} + \frac{\partial pCO_2}{\partial A_T}\frac{dA_T}{dt} \qquad (6)$$

$$\frac{dpCO_2}{dt} = \frac{\partial pCO_2}{\partial SST}\frac{dSST}{dt} + \left(\frac{\partial pCO_2}{\partial SSS} + \frac{NC_T}{SSS_0}\frac{\partial pCO_2}{\partial C_T} + \frac{NA_T}{SSS_0}\frac{\partial pCO_2}{\partial A_T}\right)\frac{dSSS}{dt} + \frac{SSS}{SSS_0}\frac{\partial pCO_2}{\partial C_T}\frac{dNC_T}{dt} + \frac{S}{S_0}\frac{\partial pCO_2}{\partial A_T}\frac{dNA_T}{dt} \qquad (7)$$

It is important to remark that the changes in NA_T and NC_T are linked with biogeochemical processes which have different influences: the processes involved in the organic carbon pump contribute to strongly change the NC_T weakly affecting the NA_T, while those involved in the carbonate pump affect the NA_T twice as much as NC_T.

2.3.4. Air-sea CO_2 fluxes

The CO_2 fluxes (FCO_2) were determined using Eq. 8 with a conversion factor of 0.24 mmol m^{-2} d^{-1}. The solubility (*S*) and the difference between seawater and low atmosphere fCO_2 ($\Delta fCO_2 = fCO_{2,sw} - fCO_{2,atm}$) were considered. Negative fluxes indicate that the ocean acts as an atmospheric CO_2 sink, while the positive ones indicate that it behaves as a source.

$$FCO_2 = 0.24 \cdot S \cdot k \cdot \Delta fCO_2 \qquad (8)$$

https://doi.org/10.5194/egusphere-2024-2709
Preprint. Discussion started: 7 October 2024
© Author(s) 2024. CC BY 4.0 License.

The Wanninkhof (2014) parameterization was used in this study, with *k* being the gas transfer rate expressed in Eq. 9:

$$k = 0.251 \cdot \mathrm{w}^2 \cdot \left(\frac{\mathrm{Sc}}{660}\right)^{-0.5} \quad (9)$$

where *w* is the wind speed (m s^{-1}) and *Sc* is Schmidt number (cinematic viscosity of seawater, divided by the gas diffusion coefficient). Both *S* and *Sc* were calculated with the equations and coefficients given by Wanninkhof (2014) for CO_2 in seawater. ERA5 hourly wind speed reanalysis data at 10 m above the sea level and with a spatial resolution of 0.25º x 0.25º (Hersbach et al., 2023) were used to calculate *k*. The ERA5 reanalysis for the global climate and weather is available at Copernicus Climate Data Store (https://cds.climate.copernicus.eu/).

2.4. Data adjustments and statistical procedures

The raw output data was initially filtered removing data affected by the automatic sampler such as samples measured at low water rates (< 2.0 L min^{-1}) and/or samples in which the difference in temperature between the seawater intake and the equilibrator was higher than 1.5ºC. The outliers, assumed as elements more than three local standard deviations from the local mean over a window length of fifty elements, were also removed from the dataset. The xCO_2 measured values in low atmosphere after each calibration were averaged and interpolated at the times of each xCO_2 observation in seawater by applying a piecewise polynomial-based smoothing spline.

The temporal evolution of the physico-chemical data was analysed by weekly averaging (time required by the vessel to complete a trip) at different locations along the vessel track. The average values (y) were fitted to Eq. 10 as a function of time (year fraction). This equation update the one used to study seasonal cycles by Curbelo-Hernández et al., (2021a; 2021b) through the addition of the $b\ (year - 2019)$ term, which provides the interannual rate of change of each seasonally-detrended variable between 2019 and 2024. The coefficients *a*-*f* and the standard errors of estimate given by Eq. 10 for the variables considered are available in Table Sup1.

$$\mathrm{y} = \mathrm{a} + b\ (year - 2019) + \mathrm{c} \cdot \cos(2\pi\ \mathrm{year}) + \mathrm{d} \cdot \sin(2\pi\ \mathrm{year}) + \mathrm{e} \cdot \cos(4\pi\ \mathrm{year}) + \mathrm{f} \cdot \sin(4\pi\ \mathrm{year}) \quad (10)$$

https://doi.org/10.5194/egusphere-2024-2709
Preprint. Discussion started: 7 October 2024
© Author(s) 2024. CC BY 4.0 License.

The errors in the weekly averages were determined by dividing the Standard Deviation by the square root of the number of data points used to calculate the means ($Standard\ Deviation/\sqrt{n}$). The coefficient b in Eq. 10 represented the interannual variation rates for each variable, which coincided with the slope derived from linear regressions of the detrended average values over time. The standard errors of these slopes were calculated by propagating the errors from the annual mean values.

To evaluate the strength and direction of the linear regressions and the significance of the interannual trends, we applied the Pearson correlation test. This test yielded correlation coefficients (r^2) and corresponding p-values to determine statistical significance. Trends with p-values ≤ 0.01 were statistically significant at the 99% confidence level, those with p-values ≤ 0.05 were significant at the 95% confidence level, and trends with p-values ≤ 0.1 were significant at the 90% confidence level. Trends with p-values > 0.1 were not statistically significant but still provided an estimate of the temporal evolution of the variables within their respective layers.

3. Results

3.1. Spatial distribution of the surface physicochemical properties.

The surface underway monitoring allowed a high-resolution characterization of the western boundary of the Mediterranean Sea. A total amount of 157,984 data for surface ocean xCO_2 were collected during the study period (34,015 data during 2019, 28,590 data during 2020, 33,288 data during 2021, 19,102 data during 2022, 39,738 data during 2023 and 3,251 data during January and February 2024). Based on differences in the spatial distribution of the observation-based data and in the heterogeneous influence of hydrodynamical processes and oceanographic features, two subregions (referred to as sections) were identified along the vessel track (Figure 1): the longitudinally distributed southern section (hereinafter S section), accomplishing the Alboran Sea (~2-5.1ºW), and the latitudinally distributed east section (hereinafter E section), following the eastern coastline of the Iberian Peninsula (~36.5-41.3ºN).

The spatial distribution of the average values allowed to identify heterogeneity in the annual cycle of each variable along the longitudinal S section and latitudinal E section (Figure 2 and Sup1). The standard deviation of the spatially-averaged variables is

https://doi.org/10.5194/egusphere-2024-2709
Preprint. Discussion started: 7 October 2024
© Author(s) 2024. CC BY 4.0 License.

presented in Table Sup2. A strong west-to-east increasing gradient in SST was observed in summer through the S section (~5.5ºC) which lead an increment in $fCO_{2,sw}$ of ~57.5 µatm and a depletion in pH of ~0.040 units from the Strait of Gibraltar to the Cape of Gata. Despite the approximately constant SST through the S section during the rest of the year (less than 1.5ºC of difference between the western and easternmost parts), an eastward decrease in $fCO_{2,sw}$ of less than 18 µatm accompanied by an increase in pH of less than 0.030 units was observed between October and March.

The latitudinal gradient of SST through the E section was weaker throughout the year, keeping spatially stables the $fCO_{2,sw}$ and pH. The maximum change in SST occurs during winter, in which a northward decrease of less than 2ºC explained minimum seasonal average temperatures and $fCO_{2,sw}$ through the cruise track (14-15 ºC and 350-360 µatm, respectively). It contrasts with the maximum average temperatures and $fCO_{2,sw}$ encountered during summer (25.0-26.5 ºC and 450-470 µatm, respectively). These results reported that the maximum amplitude of the seasonal cycle of SST, $fCO_{2,sw}$ and pH occurs along the eastern coastline of the Iberian Peninsula and specially over the continental shelf between Valencia and Barcelona (northernmost part of E section), while the minimum seasonal amplitude occurs near the Strait of Gibraltar (westernmost part of the S section).

The spatial variation in C_T (Figure 2) were significant throughout the year along both sections in phase with the distribution of A_T and the strong gradient in SSS (Figure Sup1). The C_T increases eastward in the order of 20-45 µmol kg^{-1} in the Alboran Sea throughout the year. This increment accelerated from Cape of Gata to Cape of Nao, where the average C_T become approximately stable until Barcelona. The spatial distribution of C_T and A_T was highly influenced by the progressively salinification observed in the semi-enclosed transitional area between the Strait of Gibraltar and the Mediterranean Sea. The SSS increased during the entire annual cycle from 36.3-36.5 around the eastern part of the Strait of Gibraltar to 37.7-38.1 around Cape of Nao (Figure Sup1). Removing the effect of salinity, the NC_T (Figure Sup1) presents a weaker spatial variation through the vessel track mainly lead by biological and mixing processes.

3.2. Seasonal cycle of the SST, SSS and MCS.

https://doi.org/10.5194/egusphere-2024-2709
Preprint. Discussion started: 7 October 2024
© Author(s) 2024. CC BY 4.0 License.

The surface physico-chemical properties show heterogeneities during some seasons of the year among several key locations along the sections (Figure 2 and Sup1). The heterogeneities in the temporal evolution of the SST, SSS and CO_2 system variables was assessed by the strategic selection of 5 stations along the S section (stations S1-S5) and 6 stations along the E section (stations E1-E6), geographically depicted in Figure 1. The S1 (4.95 ± 0.05 ºW) occupied the easternmost part of the Strait of Gibraltar, the S2-S4 (4.35 ± 0.05 ºW, 3.85 ± 0.05 ºW and 2.95 ± 0.05ºW) were placed in the central Alboran Sea and the S5 (2.45 ± 0.05 ºW) located south of Cape of Gata. The stations along the E section include E1 (37.1 ± 0.2 ºN) in the Gulf of Mazarron, E2 (37.6 ± 0.2 ºN) to the east of Cape of Palos, E3 (38.2 ± 0.2 ºN) in the Gulf of Alicante, E4 (38.7 ± 0.2 ºN) to the east of Cape of Nao, E5 (39.3 ± 0.2 ºN) in the Gulf of Valencia over the continental slope, and E6 (40.2 ± 0.2 ºN) near the Ebro estuary over the continental shelf.

The temporal variations of each variable at S1-S5 and E1-E6 are depicted in Figure 3, 4, Sup2, Sup3 and Sup4. The seasonal amplitudes and interannual trends are summarized in Table 1. The seasonal amplitude of SST (minimum values in February-March around 14-17 ºC and maximum values in August-September around 20-26ºC) increased eastward through the S section although the local decrease at S2 (Figure 3 and Sup2, Table 1). The seasonal changes were larger through the E section (~14 to ~28ºC) and show weaker spatial variations (Figure 4 and Sup3, Table 1). The SSS (Figure Sup4), do not exhibit a seasonal cycle well-correlated to the harmonic function Eq. 10 ($r^2 < 0.5$; Table Sup2). The lower and more spatially stable SSS values were observed along the S section during the entire period (around 36.0-37.5), while increase with latitude through the E section (around 36.7-38.1).

The seasonal amplitude of $fCO_{2,sw}$ (from ~340 to ~460 µatm in the S section and from ~340 to ~470 µatm in the E section) and pH (from ~8.00 to ~8.12 units in the S section and from ~8.00 to ~7.98 to ~8.13 units in the E section) was strongly linked with those of SST. It exhibits a west-to-east increment through the S section with the exception at S2 (Figure 3 and Sup2, Table 1) and remained approximately constant through the E section (Figure 4 and Sup3, Table 1). These spatial heterogeneities in the seasonal cycles were found to be leaded by the different rise in SST during late summer along each section as minimal spatial differences were observed during the rest of the year.

https://doi.org/10.5194/egusphere-2024-2709
Preprint. Discussion started: 7 October 2024
© Author(s) 2024. CC BY 4.0 License.

The C_T (Figure Sup4) seasonally decreased from January-February to September-October (from ~2180 to ~2085 µmol kg^{-1} in the S section and from ~2260 to ~2105 µmol kg^{-1} in the E section) in phase with the enhancement biological production. The seasonal amplitude of C_T increased eastward through the S section and northward through the E section, following the salinification gradient (Figure Sup4, Table 1). Once removed the effect of salinity, the seasonal cycle of NC_T shows minimal differences in the S section between the western and the easternmost part, while in the E section the NCT and its seasonal amplitude continued to northward increase (Figure Sup4, Table 1). The enhanced adjustment (correlation) of NC_T with Eq. 10 ($0.47<r^2<0.61$ at S section and $0.70<r^2<0.88$ at E section) compared to C_T ($0.28<r^2<0.56$ at S section and $0.45<r^2<0.73$ at E section) emphasizes the relevance of the salinity-dependent processes. The lower correlations encountered through the S section shows the higher impact of eventual processes (i. e. changes in the evaporation/precipitation, river runoff, mesoscale features) locally modifying the surface carbon system in this area and introducing spatial heterogeneities in their seasonal cycles.

4. Discussion

4.1. Spatial characterization of the CO_2 system and its seasonality

The observation-based data allows to evaluate, with high spatio-temporal resolution, the seasonal cycle of the CO_2 system together with their spatial heterogeneities in the Alboran Sea (S section) and eastern coastal transitional area of the Iberian Peninsula (E section). The seasonal cycle of the variables considered was subject to spatial variability related to the irregular coastline of the Iberian Peninsula, which caused local differences in the oceanographic features and variances in the distance-to-land of the vessel track.

The west-to-east warming and salinification of MAW while entering and advancing across the Alboran Sea was found to occur mainly during summer and account to rise eastward the $fCO_{2,sw}$ and fall down the pH (Figure 2). The lowest seasonal amplitude of $fCO_{2,sw}$ was encountered in the western Alboran Sea (Figure 3). During the late-winter, the AMI reaches its shallowest position and feed the surface with CO_2-rich waters coming from deeper areas in the Mediterranean Sea (De La Paz et al., 2009; Echevarría et al., 2002; Gómez-Jakobsen et al., 2019; Minas et al., 1991), elevating $fCO_{2,sw}$ around S1 in comparison to adjacent waters (Figure 2 and 3). During summer, the wind-induced upwelling along the northern coast of the western Alboran Sea cooled the surface and

https://doi.org/10.5194/egusphere-2024-2709
Preprint. Discussion started: 7 October 2024
© Author(s) 2024. CC BY 4.0 License.

enhanced the biological drawdown of $fCO_{2,sw}$ and in C_T (e. g. Bolado-Penagos et al., 2020; Folkard et al., 1997; Gómez-Jakobsen et al., 2019; Peliz et al., 2009; Richez and Kergomard, 1990; Stanichny et al., 2005).

The seasonal variability of the AJ (García-Lafuente et al., 2002; Macías et al., 2008, 2016; Vargas-Yáez et al., 2002) modified the SST signature (Figure 1b) influencing $fCO_{2,sw}$ and pH in the Alboran Sea. The high-intensity of the AJ feeding the two-gyres configuration during summer (Peliz et al., 2013; Renault et al., 2012) introduced larger spatial changes compared to the rest of the year. The vessel tracks longitudinally crossed the WAG through its northern part and followed the northern path of the EAG. The signal of the summer AJ surrounding the northern part of the WAG (Figure 1b) was observed in local minimum values of SST and $fCO_{2,sw}$ (Figure 2) at S1 (20.68 ± 2.20 ºC and 401.68 ± 27.13 µatm) and S3 (21.15 ± 2.11 ºC and 407.30 ± 26.20 µatm), which increased toward the core of the WAG at S2 (22.63 ± 2.05 ºC and 429.98 ± 24.86 µatm). The progressively cooling and decrement in $fCO_{2,sw}$ from S2 to S3 (Figure 2) reflects the signal of the cold and nutrient-rich filament separating the gyres (Gómez-Jakobsen et al., 2019; Millot, 1999).

The SST and $fCO_{2,sw}$ increased toward the northern path of the EAG around S4 (23.89 ± 2.03 ºC and 438.25 ± 25.22 µatm) and S5 (24.05 ± 1.61 ºC and 441.67 ± 16.22 µatm) due to the mixing of MAW with warmer MW surrounding the Cape of Gata and recirculating westward along the southern Iberian coastline (Millot, 1999; Sánchez-Garrido et al., 2013). In terms of C_T and NC_T (Figure 2 and Sup1), a weak decrement around S2 was observed between January and September and may be due to the injection of deeper waters into surface waters enhancing the biological drawdown in the core of the WAG. The C_T and NC_T continue increasing eastward S2 throughout the year as it mixed with MW.

The hydrodynamic regime of the Alboran Sea during summer with the AJ showing its maximum intensity (Figure 1b) introduces spatial heterogeneities in the seasonal cycles (Figure 2). The seasonal amplitudes of SST, $fCO_{2,sw}$ and pH (Figure 3 and Sup2, Table 1) around the WAG (at S2) and EAG (at S4) were higher than the observed over the filament separating both gyres (at S3). The opposite occurred for C_T (Figure Sup4, Table 1), which suggests that the upwelled waters transported by the filament were not enough remineralized to compensate the SST-driven decrease in $fCO_{2,sw}$ during summer.

The eastern coastal transitional area of the Iberian Peninsula was subject to variability related with changes in the intensity, morphology and path of the Northern Current (Figure 1b). During winter, the warm waters in the wind-shielded area North of Cape of Nao mixed with cool and salty MW transported by the Northern Current. It explained the observed decrease in SST of ~1.0ºC during the cold months from Sagunto to Barcelona coasts (north of S5; Figure 2). During summer, the change in the path of the Northern Current due to the formation of a thermal front in the axis of the Pyrenees (López-García et al., 1994) favoured the recent MAW to be northward spreading and to get trapped along the north-easternmost Iberian coastal area. It forms the warmest waters of the Western Mediterranean (Lopez Garcia et al., 1994; Millot, 1999) and account to reduce the observed cooling (~0.8ºC) at this time of the year (Figure 2). In the southernmost part of the section, the SST increased from Cape of Gata (at S5) to Cape of Nao (at E4) by ~1.5ºC during summer and decreased by ~0.7ºC during winter (Figure 2). The enhanced northward spreading of MAW and less wind stress during summer drive the warming, while a low intense branch of the Northern Current transporting MW and progressing southward Cape of Nao weakly cool the area during winter (López-García et al., 1994; López-Jurado et al., 1995).

The offshore recirculation of the Northern Current driven by the bathymetry and the formation of the high-intense Balearic Front during the warm months (Millot, 1999), detectable in the reanalysis-based SST map (Figure 1b), explained the local decrease in SST and $fCO_{2,sw}$ observed at E4 (Figure 2). The C_T and NC_T signatures evidenced the differences between the areas south and north of Cape of Nao (Figure 2 and Sup4). The northernmost part of the section receives remineralized MW transported by the Northern Current which elevates C_T and NC_T. Ulses et al. (2023) recently suggested that the convective area in the Gulf of Lion behaves as a source of natural and anthropogenic carbon to the intermediate waters of the western Mediterranean, which can enter the surface through vertical mixing and account for the observed high amount of C_T and NC_T. In contrast, the southernmost part was supplied with recent MAW with relatively low C_T and NC_T.

The seasonal variations were modulated by the higher stratification during the warm months and the variety of mesoscale features (mainly meanders and eddies) interacting with the most energetic Northern Current during the cold months (Bosse et al., 2021;

https://doi.org/10.5194/egusphere-2024-2709
Preprint. Discussion started: 7 October 2024
© Author(s) 2024. CC BY 4.0 License.

Millot, 1999). The seasonal amplitudes of SST and $fCO_{2,sw}$ increased northward from E1 to E6 (Figure 3 and Sup3, Table 1). The higher seasonal amplitudes occurred in the areas where the Northern Current introduces larger differences between the cold and warm months. The location of station E5, away from the influence of the Northern Current during the warm months, explained its locally lower seasonal amplitudes compared to adjacent waters. Nevertheless, these heterogeneities were minimal and do not caused differences in the seasonal amplitude of pH (Table 1). In the case of C_T and NC_T (Figure Sup4, Table 1), the enhancement in the mixing of MAW with MW during winter increased northward the seasonality from E1 to E4.

The E6 was subject to local variability related with freshwater discharge from the Ebro River interacting with the circulation pattern. The Ebro River runoff peaks in March-May due to the combined action of precipitation during winter and snowmelt in the upper river basins during spring (Zambrano-Bigiarini et al., 2011). This fed the coastal area around the Ebro Delta with low SSS and SST waters (see in minimum SST compared to adjacent waters in February; Figure 1b). The intense NAC at this time of the year further cooled this coastal area and inflowed saline water which neutralized the peak signal of freshwater discharge. During summer and fall, the low SSS signal resulted from the Ebro River runoff combined with the northward spreading of MAW. This explained the minimum seasonal differences in SSS (Figure Sup4). The approximately constant A_T and NA_T content at E6 throughout the year resulted from the interactions of freshwater fluxes with MW and MAW compensated for the seasonal variations in C_T and NC_T (Figure Sup4) expected by air-sea interactions and due to its position over the continental shelf, hence enhancing biological processes.

4.2. Warming of the Western Mediterranean Sea and interannual trends of the CO_2 system variables

The ongoing warming of the surface Western Mediterranean Basin and its impact on the marine carbonate dynamics were assessed. The interannual trends are shown in Table 1 and 2. During 2019-2024, the SST increased at a rate of 0.38 ± 0.05 ºC yr^{-1} in the S section and 0.30 ± 0.04 ºC yr^{-1} in the E section. The rate of increase in SST locally intensified at S2 (0.50 ± 0.09 ºC yr^{-1}) may be due to the transport and accumulation of surface waters toward the core of the WAG. Its variability, migration and progressively collapse can also account for the rapid warming of the area (Sánchez-Garrido et al., 2013; Viúdez et al.,

https://doi.org/10.5194/egusphere-2024-2709
Preprint. Discussion started: 7 October 2024
© Author(s) 2024. CC BY 4.0 License.

1998; Vélez-Belchí et al., 2005). Interannual trends were also computed for SST reanalysis monthly data (0.042º x 0.042º; with dates spanning 24 years within 01/01/2000 and 01/03/2024) from the Med MFC physical multiyear product (Escudier et al., 2020; 2021; Nigam et al., 2021), available at Copernicus Marine Data Store (https://data.marine.copernicus.eu/products). The SST reanalysis data was interpolated to the coordinates of the CanOA-VOS data. The SST trends based on CanOA-VOS data were in the same order of magnitude of those based on reanalysis data for 2019-2024. Considering the reanalysis data-based SST trends during 2000-2019 in the S section (0.046 ± 0.005 ºC yr^{-1}, p-value<0.01) and E section (0.067 ± 0.005 ºC yr^{-1}, p-value<0.01), the CanOA-VOS data-based SST trends reported a strengthening in warming during 2019-2024 of 87.9% and 78.0% in the respective subregions compared to the previous two decades. The rates of increase in SST experienced an acceleration of >97% in comparison with the extracted from the Hadley Centre HadISST1.1 dataset (Rayner et al., 2003) among the period 1950-2009 for the Atlantic and Mediterranean basin (0.007 ºC yr^{-1}; p-value < 0.01, and 0.009 ºC yr^{-1}, p-value > 0.1; respectively; Hoegh-Guldberg et al., 2014).

The CanOA-VOS data-based interannual SST trends were found to be reinforced during summer by 55.2% in the S section and by 32.4% in the E section (0.60 ± 0.20 and 0.29 ± 0.10 ºC yr^{-1}, respectively; p-values < 0.01) compared to winter (0.26 ± 0.04 and 0.20 ± 0.05 ºC yr^{-1}, respectively; p-values < 0.01). The Northern Current cooled the northernmost part of the E section and accounted to decelerate the warming in comparison to the S section. These trends enhanced the comprehension of the stronger warming during the warm season compared to the cold season, as the reanalysis data-based trends for the same period were not statistically significant (p-values > 0.1). In addition, they represent an increment in warming of 81-84% respect to 2000-2019 (0.10 ± 0.03 ºC yr^{-1}, p-value < 0.05, in the S section; and 0.06 ± 0.03 ºC yr^{-1}, p-value <0.1, in the E section). Comparisons were difficult to perform during wintertime as non-significant trends were identified for 2000-2019 (p-values > 0.1). These results emphasized the relevant role of the large increase in SST during the warm season on the progressing acceleration in warming. It aligns with projections from climate models for both terrestrial and marine environments in the mid latitudes, particularly within the Mediterranean region, in consequence of human-induced global warming, which was detailed by Hoegh-Guldberg et al., (2018) in the AR6 Synthesis Report (IPCC, 2023). The CanOA-VOS data-based

https://doi.org/10.5194/egusphere-2024-2709
Preprint. Discussion started: 7 October 2024
© Author(s) 2024. CC BY 4.0 License.

interannual SST trends reported an increase in SST during the study period of 1.91 ± 0.26 ºC in the Alboran Sea and 1.52 ± 0.22 ºC along the eastern Iberian coastal transitional zone. These cumulative increments were 48.3% and 34.94% respectively higher than those estimated for the global surface ocean from 1850-1900 to 2001-2020 (0.99 ± 0.12 ºC; IPCC, 2023).

The warming contributes to modify the marine carbonate system dynamics, mainly accelerating the increase in $fCO_{2,sw}$ and acidification. The interannual trends of $fCO_{2,sw}$ and pH (Table 1) were more than twice (except for trends at S1) than those reported for the Northwestern Mediterranean at the DYFAMED site based on the difference between average data for the periods 1995-1997 and 2013-2015 (2.30 ± 0.23 µatm yr^{-1} and -0.0022 ± 0.0002 units yr^{-1}; Merlivat et al., 2018) and for the Northeast Atlantic at the ESTOC site based on in situ measurements since 1995 (2.1 ± 0.1 µatm yr^{-1} and 0.002 ± 0.0001 units yr^{-1}, respectively; González-Dávila and Santana-Casiano, 2023). The interannual rates accelerated eastward along the S section and northward along the E section (Table 1). The stronger trends at S3 compared to adjacent waters (S2 and S4) may be due to the transport of CO_2-rich waters from the southern Iberian coast through the filament. The trends in the S section were conducted by the larger rates of change encountered during the warm season compared to the cold season. The opposite occurred in the E section, where an intense increase in $fCO_{2,sw}$ accompanied by a drawdown in pH occurred during winter and trends were reversed during summer (Table 1).

These spatial differences among the cold and warm seasons were mainly linked with variations in the biological production/remineralization and mixing and were independent of the surface ocean warming. Hence, they were required to be assessed together with the NC_T trends for a better understanding. The NC_T interannually decreases throughout the region (Table 2). The rapid depletion in the S section during winter in comparison to summer could be due to first, an interannual weakened in remineralization processes and/or inputs of CO_2-rich water to the area during the cold months, and second, an interannual strengthened in the biological uptake during the warm months. However, these variations resulted insufficient to compensate the increase in $fCO_{2,sw}$ and subsequent fall down in pH induced by warming during the cold and even more during the warm months. Conversely, in the E section, the variations in lateral/vertical advection, primary driven variations in the (sub)mesoscale structures (Alberola et al., 1995; Bosse et al.,

https://doi.org/10.5194/egusphere-2024-2709
Preprint. Discussion started: 7 October 2024
© Author(s) 2024. CC BY 4.0 License.

2021; 2016; Bourg and Molcard, 2021), were of high-relevance and introduced differences in the annual cycle of NC_T. The interannual variations during winter (Table 1, Figure Sup4) were minimal likely due to not significant changes in remineralization and in the dissolved CO_2 concentration of waters transported into the area. The decrease in NC_T intensified during summer (Table 1, Figure Sup4) likely caused by the enhancement in biological production together with the dismissing lateral advection (this may be related with a reinforcement in the front formed in the axis of the Pyrenees due to the increasingly higher SST of the MAW).

Once removed the effects of temperature, the interannual pH_{19} trends overturned to negligible and were not statistically significant in the S section (<-0.001 units yr^{-1}; p-values > 0.1). It suggest that warming is directly and indirectly (by rising the $fCO_{2,sw}$) driving the acidification while the progressively enhancing in biological productivity compensates for the expected fall down in pH driven by rising atmospheric CO_2. In the E section, pH_{19} were reduced by 63% (-0.002 ± 0.001 units yr^{-1}; p-values < 0.01) in comparison to the pH trends, which explains that the increase in SST is contributing more than half on the acidification due to only the atmospheric fCO_2 increase. The negative pH_{19} trends reinforced in the E section by 47% during the cold season due to the enhancement in remineralization. The pH_{19} trends reversed to positive during the warm season due to the important role of biological production actively reducing $fCO_{2,sw}$ and rising pH at this time of the year. This remarked the relevant role of non-thermal processes occurring during the cold season and contributing to the acidification trends on an interannual scale (see below)

However, despite the high statistical confidence in the trends and the consistency found with reanalysis products, the acceleration in surface warming and consequent changes in $fCO_{2,sw}$ and pH observed may be linked to isolated extreme events such as marine heat waves and are not necessarily indicative of prolonged behaviours over time. The globally increased frequency and magnitude in marine heat waves in phase with warming (Oliver et al., 2018; Hoegh-Guldberg et al., 2018; Frölicher et al., 2018; Smale et al., 2019) could feedback and hence continue expediting the ocean warming. The influence of these extreme events is especially relevant in semi-enclosed seas as the Mediterranean, recognized as one of the most affected marine areas as yearly mentioned in the

https://doi.org/10.5194/egusphere-2024-2709
Preprint. Discussion started: 7 October 2024
© Author(s) 2024. CC BY 4.0 License.

Copernicus Ocean State Reports (OSR; EU Copernicus Marine Service; https://marine.copernicus.eu/access-data/ocean-state-report) since 2016 (OSR1-OSR7).

4.3. The relative contribution of thermal and non-thermal processes on the surface $fCO_{2,sw}$

The relative influence of thermal and non-thermal processes on the $fCO_{2,sw}$ variations at seasonal and interannual scales were addressed following the procedures of Takahashi et al. (2002) and Fassbender et al. (2022), hereinafter referred as T'02 and F'22, respectively. Its temporal evolution is depicted in Figures 3 and 4 and show the high coincidence between both methodologies. The average $fCO_{2,sw}$ explained by thermal and non-thermal processes ($fCO_{2,T}$ and $fCO_{2,NT}$, respectively) presented differences lower than 5 µatm between T'02 and F'22 (Table 2). The consistency with the widely employed T'02 engenders confidence in the validity and reliability of the most updated F'22 method.

The seasonal amplitudes and interannual trends of $fCO_{2,T}$ and $fCO_{2,NT}$ are presented in Table 2. The thermal-driven seasonal changes ($dfCO_{2,T}$) were found to approximately double those independent of temperature ($dfCO_{2,NT}$) throughout the region. The seasonal variations were close to twice in the E section compared to the S section. The T/B ratios (Table 2) demonstrated the control of thermal processes over the seasonality of $fCO_{2,sw}$ throughout the region. The T/B ratios in the westernmost part of the S section (between 1 and 2) were consistent with previous studies in the Strait of Gibraltar (Curbelo-Hernández et al., 2021; De La Paz et al., 2009). The T/B ratios increased eastward as the AJ advanced in the Alboran Sea and caused by the intense increase in $dfCO_{2,T}$ compared to $dfCO_{2,NT}$. They exceeded 2 in S4-S5 and E1-E6, which demonstrated the larger control of SST over $fCO_{2,sw}$ in areas less influenced by incoming of surface Atlantic water

The interannual trends show the control of thermal processes over the increase in $fCO_{2,sw}$ during 2019-2024 (Figure 3 and 4; Table 2). The strong and statistically significant interannual $fCO_{2,T}$ trends show the important role of warming in elevating $fCO_{2,sw}$. The weak and non-significant $fCO_{2,NT}$ trends suggest that spatio-temporal variations in the biological processes, circulations patterns and air-sea gas exchange introduced local differences in the distribution of $fCO_{2,sw}$. It difficult to assess the impact of the non-thermal processes on an interannual scale at each of the stations. The interannual trends

https://doi.org/10.5194/egusphere-2024-2709
Preprint. Discussion started: 7 October 2024
© Author(s) 2024. CC BY 4.0 License.

of $fCO_{2,T}$ and $fCO_{2,NT}$ for the entire S and E sections (Table 2) were statistically significant at more than the 95% level of confidence and its coupling described, with less than 0.3 µatm yr^{-1} of difference (<1%), the interannual rates of $fCO_{2,sw}$ during 2019-2024 (Table 1; section 4.2).

The thermal processes govern the changes in $fCO_{2,sw}$ on an interannual scale with a contribution ranged between ~76-92% in the S section and ~73-83% in the E section. The contributions for $fCO_{2,NT}$ were between ~8-25% and ~17-27%, respectively. The decrease in $fCO_{2,NT}$ compensated by ~6-30% the increase in $fCO_{2,sw}$ at S1-S5 and E1-E2, while its increase contributed by ~24-53% to rise $fCO_{2,sw}$ at E3-E6. The negative $fCO_{2,NT}$ trends in the S section were related to progressive enhancement in the biological uptake (mainly during spring/summer) not compensated by remineralization and/or vertical/lateral advections of remineralized waters (mainly during autumn/winter) in areas influenced by recent MAW. Conversely, the interannual increase in $fCO_{2,NT}$ in the E section suggest that the supply of cool and remineralized MW along the path of the high-intense Northern Current surpasses the biological drawdown of surface CO_2 and is accounting to accelerate the increase in $fCO_{2,sw}$ on an interannual scale.

4.4.Mechanism controlling the seasonality of $fCO_{2,sw}$

The partial contribution of the individual component controlling the seasonal cycle of $fCO_{2,sw}$ was assessed. The seasonal rates of change of $fCO_{2,sw}$ ($\frac{dfCO_{2,sw}}{dt}$, hereinafter $dfCO_2$) explained by fluctuations in SST ($\frac{\partial fCO_{2,sw}}{\partial SST}\frac{\partial SST}{dt}$, hereinafter $dfCO_2^{SST}$), SSS ($\frac{\partial fCO_{2,sw}}{\partial SSS}\frac{\partial SSS}{dt}$, hereinafter $dfCO_2^{SSS}$), A_T ($\frac{\partial fCO_{2,sw}}{\partial A_T}\frac{\partial A_T}{dt}$, hereinafter $dfCO_2^{AT}$) and C_T ($\frac{\partial fCO_{2,sw}}{\partial C_T}\frac{\partial C_T}{dt}$, hereinafter $dfCO_2^{CT}$) were calculated for each year using Eq. 7 (section 2.3.3) at S1-S5 and E1-E6 and depicted in Figure 5. The positive values indicate an increase in $fCO_{2,sw}$ from February to September, while negative values the opposite.

The SST was identified as the main driver of $dfCO_2$, describing 45-78% and 55-83% of its changes in the S and E sections, respectively. In the S section (Figure 5a), $dfCO_2^{SST}$ increased westward as MAW get warmed in the Alboran Sea, while the incursion of the filament locally cooled the surface and decreased $dfCO_2^{SST}$ at S3. In the E section (Figure 5b), $dfCO_2^{SST}$ increased northward and reach its maximum north of Cape of Nao (at E4-

https://doi.org/10.5194/egusphere-2024-2709
Preprint. Discussion started: 7 October 2024
© Author(s) 2024. CC BY 4.0 License.

E6), particularly during 2021-2022 (32.0-32.5 µatm month^{-1}), due the higher influence of warmed MW.

The A_T has a low influence on increasing d$f$$CO_2$ in the entire region (<15%). As the $fCO_{2,sw}$ inversely changes with A_T, the weakly negative dfCO_2^{AT} found for some years along the S section show fluctuations in the periods of increment and decrement of A_T likely related with changes in the mixing processes. The A_T contribution becomes negligible at E6 (<1%) due to the minimal seasonal amplitude of A_T and NA_T (Figure Sup4). The approximately constant A_T and NA_T levels throughout the year may be due to the bicarbonate and carbonate content from the Ebro River runoff being neutralized by those in MW and MAW, which spread into the area during winter and summer, respectively. dfCO_2^{AT} tend to decrease since 2020-2021 in S1-S3, S5 and E1 due to the progressively weakening in the NA_T depletion from February to September. The opposite occurred north of Cape of Palos, where the seasonal cycle of NA_T reaches its maximum amplitude (20-27 µmol kg^{-1} at E3 and E4). The interannual dealkalinization in S and E sections (Table 1) behaves as a source of heterogeneities: the interannual negative NA_T trends during the cold months (p-values < 0.01) were stronger than during the warm months (p-values > 0.1) and consistent in both sections. The spatial differences in the summer trends (weaker in the S compared to E section) account for an enhanced reduction of the seasonal amplitude of NA_T in the S section.

The dfCO_2^{SSS} were minimal in both the S and E sections (<0.7 and < 1.9 µatm month^{-1}, respectively) and show the weak impact of SSS over dfCO_2 (<3.5%). The entrance of MAW and its mixing with saltier MW in the Alboran Sea do not allow to identify a seasonal pattern in SSS (Figure Sup4), thus explained the negligible contribution of SSS in the S section (~2.3% at S1 which fall down to <1.0% at S2-S5). The larger seasonal amplitudes of SSS at E1-E5 (Figure Sup4) led a relatively major influence of SSS (~1.0-2.4% during most of the years). The low seasonal amplitude of SSS and A_T at E6, likely related with an approximately constant influence of the Northern Current at this location throughout the annual cycle, caused a minimal variation in dfCO_2 (<1%).

The depletion in C_T, mainly drove by the increased biological production from February to September, had a significant impact on dfCO_2 (25-38%). It compensates more than one third of the expected increase in dfCO_2 driven by SST and slightly prompt by A_T. In the S section (Figure 5a), the lower changes observed during the period of study in dfCO_2^{CT}

https://doi.org/10.5194/egusphere-2024-2709
Preprint. Discussion started: 7 October 2024
© Author(s) 2024. CC BY 4.0 License.

(4-6 µatm month^{-1}) compared to d$f CO_2^{SST}$ (6-9 µatm month^{-1}) demonstrated that fluctuations in C_T were increasingly insufficient to counterbalance the warming-driven increase in dfCO_2, even at S2-S4 where the biological production enhanced and hence the dfCO_2^{CT} reinforced since 2020. In the westernmost part of the S section, the influence of C_T offsetting dfCO_2 was maximum during 2019-2020 at S1 (>84%), S2 (67.3%) and S3 (86.1%) and diminished toward 2023 (37.1%, 38.3% and 45.1%, respectively). In the easternmost part, this compensation was around 33-44% at S4-S5 throughout the period (as at S2 and S3 since 2020) except for 2023 at S5, in which dfCO_2^{CT} weakened and offset only the 22.8%. In the E section (Figure 5b), the progressively strength in the processes depleting C_T throughout the period at E1-E4 and since 2020 at E5-E6 compensated by 33-46% the dfCO_2^{SST}, which changes inversely to dfCO_2^{CT}. The lowest compensation found in 2019 at E5 (28.8%) and E6 (18.4%) was likely related with isolated eventual improved injections of remineralized waters along the Northern Current path, which offset the biological uptake of C_T and elevated the dfCO_2^{CT}.

4.5. Air-sea CO_2 exchange across the Western Boundary of the Mediterranean Sea

The Eastern Boundary of the Mediterranean Sea was characterized for the first time in terms of air-sea CO_2 exchange. The variability of FCO_2 was governed by fluctuations in ΔfCO_2 (Figure 6), mainly controlled by the larger range of variation of $fCO_{2,sw}$ (325-500 µatm) compared to $fCO_{2,atm}$ (390-425 µatm). The SST fluctuations has a relevant role by primary controlling $fCO_{2,sw}$ (section 4.3) and modulating the solubility of CO_2 at the air-sea interface, while the changes in the wind speed influence the gas transfer velocity (Wanninkhof, 2014).

The entire monitored area was undersaturated for CO_2 respect to the low atmosphere between late October and June (ΔfCO_2= -35.30 ± 8.97 µatm), acting as an atmospheric CO_2 sink (-2.56 ± 0.55 mmol m^{-2} d^{-1}) which peaks in winter (-4.53 ± 0.44 and -3.29 ± 0.31 mmol m^{-2} d^{-1} in S and E sections, respectively). During summer, the area was supersaturated for CO_2 (ΔfCO_2= 36.43 ± 0.35 µatm) and acted as a source, which was about three times more intense along the E section (1.70 ± 0.43 mmol m^{-2} d^{-1}) compared to the S section (0.57 ± 0.35 mmol m^{-2} d^{-1}). The spatial differences in SST during warm months introduced heterogeneities in the seasonal outgassing among both sections: the higher SST during summer in the E section reduced the solubility and contributed to a

https://doi.org/10.5194/egusphere-2024-2709
Preprint. Discussion started: 7 October 2024
© Author(s) 2024. CC BY 4.0 License.

higher increase in $fCO_{2,sw}$ respect to $fCO_{2,atm}$ (ΔfCO_2= 49.83 ± 0.32 µatm) compared to the cooler S section (ΔfCO_2= 16.35 ± 0.14 µatm). The seasonality in the formation of the CO_2 sink and source in the Alboran Sea was consistent with previous studies in the Strait of Gibraltar (Curbelo-Hernández et al., 2021; de la Paz et al., 2011, 2009) and Northwest African coastal transitional area in the Northeast Atlantic (Curbelo-Hernández et al., 2021b; Padin et al., 2010) and agreed with the seasonal pattern characteristic for tropical and subtropical regions (Bates et al., 2014; Takahashi et al., 2002). The warming during summer at S1 was insufficient to led supersaturated conditions (ΔfCO_2= -5.56 ± 0.26 µatm) and thus acted as a CO_2 sink throughout the year (-2.83 ± 1.77 mmol m^{-2} d^{-1} during cold months and -0.52 ± 0.02 mmol m^{-2} d^{-1} during the warm months), which coincided with the behaviour observed in the Strait of Gibraltar during 2019 (Curbelo-Hernández et al., 2021). The sink and source status during cold and warm months encountered in the Eastern Iberian Margin agreed with FCO_2 evaluations based on observations in the Mediterranean basin through its northwestern (Wimart-Rousseau et al., 2023, 2021, 2020) and eastern parts (Sisma-Ventura et al., 2017), and confirms previous estimations based on satellite data and models (D'Ortenzio et al., 2008; Taillandier et al., 2012).

The variations in FCO_2 during the period of study were addressed by averaging the data across seasons and years at each of the selected stations (Figure 7). The same procedure was applied to ΔfCO_2 and wind speed (Figure Sup5 and Sup6). The evolution of the seasonal ingassing and outgassing was evaluated by computing interannual trends for average FCO_2 and ΔfCO_2 (Figure 7). The interannual FCO_2 trends evidenced the progressively strength of the summer source in the S section, which was accelerated at S2 in response to the enhanced warming around the WAG (detailed in section 4.2) and at S4-E1 due to their exposition to increasing wind forcing (Figure Sup5 and Sup6). It was caused by the increase in $fCO_{2,sw}$ during the warm months not offset by biological drawdown which elevated ΔfCO_2. In contrary, the localization of E2-E6 over the eastern Iberian continental shelf and slope allowed the relevant biological uptake at this time of the year to compensate for the influx of CO_2-rich water. It introduced heterogeneities in ΔfCO_2 between years which do not allow to identify statistically significant trends.

During spring and autumn, the increase in ΔfCO_2, mainly driven by warming, accompanied by the decreasing wind stress (Figure Sup5 and Sup6), led the positive interannual FCO_2 trends at S2-S5 and E1-E6 (Figure 7). They show the weakening in the

© Author(s) 2024. CC BY 4.0 License.

ingassing during autumn and the achievement of a near-equilibrium state with the atmosphere during spring by the end of the study period. The FCO_2 reversed to weakly positive during spring 2023 in the E section, which prolonged the seasonal source period having a relevant impact on the net annual FCO_2. During winter, the increasing wind forcing compensated the reduction in the ingassing expected by the rise in ΔfCO_2 (Figure Sup5 and Sup6). However, the variability in the wind speed and other processes involved in the non-thermal change of $fCO_{2,sw}$ between years does not allowed the identification of statistically significant rates of change in the CO_2 sink status. Particularly, the relatively high wind speed during winter 2021 may have contributed to accelerated horizontal transports, increasing $fCO_{2,sw}$ and hence ΔfCO_2 (Figure Sup5 and Sup6).

The predominantly negative FCO_2 during most of the year led a net annual CO_2 sink behaviour. The positive FCO_2 trends during summer, spring and autumn have forced the annual average CO_2 invasion to decrease by 44-65% at S2-S5 (ranging from -0.66 ± 0.06 and -0.84 ± 0.04 mol m^{-2} during 2019 to -0.27 ± 0.09 and -0.47 ± 0.09 mol m^{-2} during 2023) and by 60-80% at E1-E6 (ranging from -0.32 ± 0.09 and -0.53 ± 0.09 mol m^{-2} during 2019 to -0.11 ± 0.10 and -0.13 ± 0.09 mol m^{-2} during 2023). The unique hydrodynamic of the Strait of Gibraltar strongly influenced the air-sea CO_2 exchange at S1: the ingassing during summer partially compensated for the reduction of the annual influx and resulted in a lower increase in FCO_2 (23%) from 2019 (-0.77 ± 0.02 mol m^{-2} yr^{-1}) to 2023 (-0.60 ± 0.06 mol m^{-2} yr^{-1}).

Considering the annual average FCO_2 for the S and E section, the net ingassing have decreased at a rate of 0.11 ± 0.02 mol m^{-2} yr^{-1} yr^{-1} (p-value<0.01) in the Alboran Sea and by 0.08 ± 0.02 mol m^{-2} yr^{-1} yr^{-1} (p-value<0.01) in the Eastern Iberian Margin. It contrast with the strength of the CO_2 sink across the western Mediterranean basin recently reported by Zarghamipour et al., (2024) for 1984-2019 based on a combination of observational data and model simulations (0.007 ± 0.001 mol m^{-2} yr^{-1} yr^{-1}). Additionally, Zarghamipour et al., (2024) noted the reduction of the annual net CO_2 source behaviour of the Central Mediterranean basin at an estimated rate of 0.003 ± 0.001 mol m^{-2} yr^{-1}. The findings suggest that the acceleration in the increase in $fCO_{2,sw}$ induced by the rapid warming, together with the progressive reduction in solubility, is reversing the interannual FCO_2 trends compared to previous decades, may be causing the study area to be resemble the Central and Eastern Mediterranean basin in terms of air-sea CO_2 exchange. The reduction

https://doi.org/10.5194/egusphere-2024-2709
Preprint. Discussion started: 7 October 2024
© Author(s) 2024. CC BY 4.0 License.

of the net annual invasion was consistent with previous estimations in such coastal and shelf environments across the eastern tropical and subtropical South Atlantic during 2002-2018 (between 0.03 ± 0.01 and 0.09 ± 0.02 mol m^{-2} yr^{-1} yr^{-1}; Ford et al., 2022) and toward mid-latitudes over the Scotian Shelf (with average FCO_2 ranging from -1.7 mol m^{-2} yr^{-1} yr^{-1} in 2002 to -0.02 mol m^{-2} yr^{-1} yr^{-1} in 2006; Sisma-Ventura et al., 2017). The continuation of this decreasing rate for net annual ingassing would imply the reversion of the study area to a net annual CO_2 source behaviour before 2030.

The net CO_2 invasion was calculated by integrating the annual cycle of FCO_2 during 2019-2023. The net FCO_2 in the Alboran Sea was -1.57 ± 0.49 mol m^{-2} yr^{-1}, which represented a strength in the CO_2 sink in comparison with adjacent surface areas across the Strait of Gibraltar (between -0.82 and -1.01 mol m^{-2} yr^{-1} during 2019-2021; Curbelo-Hernández et al., 2021) and the Eastern Iberian Upwelling (-1.33 mol m^{-2} yr^{-1}; Chen et al., 2013). The net FCO_2 along the Eastern Iberian margin was -0.70 ± 0.54 mol m^{-2} yr^{-1}, which fall within the range of those modelled for the deep-convection area around the Bay of Marseille (Northwestern Mediterranean Basin) during 2012-2013 (-0.5 mol m^{-2} yr^{-1}; Ulses et al., 2023) and estimated based on observations during 2017-2018 (between -0.26 and -0.81 mol m^{-2} yr^{-1}; Wimart-Rousseau et al., 2020). However, it was opposite to the net outgassing across the Easten Mediterranean basin (0.85 ± 0.27 mol m^{-2} yr^{-1} during 2009-2015; Sisma-Ventura et al., 2017). The net CO_2 sink for the monitored area across the Alboran Sea (14,000 Km^2) and eastern Iberian margin (40,000 Km^2) was -0.97 ± 0.30 Tg CO_2 yr^{-1} (-0.26 ± 0.08 Tg C yr^{-1}) and -1.22 ± 0.95 Tg CO_2 yr^{-1} (-0.33 ± 0.25 Tg C yr^{-1}). These findings powerfully contributed to the assessment of the air-sea CO_2 exchange in the Mediterranean basin (Borges et al., 2005) and global coastal and shelf areas (Chen et al., 2013).

5. Conclusion

The five years of automatically underway observations through the CanOA-VOS line provided a high spatio-temporal resolution dataset which includes the surface physical and MCS properties across the western boundary of the Mediterranean Sea. It allowed the characterization, with an improved degree of certainty for the highly variable Alboran Sea and Eastern Iberian coastal transitional area, of patterns and mechanisms involved on seasonal and interannual timescales.

The findings reveal the influence of the upper-layer circulation patterns and subsequent physical and biological implications on the MCS. In the Alboran Sea, the high intensity of the AJ during summer warms the surface layer, driving larger seasonal changes in SST, $fCO_{2,sw}$ and pH toward the core of the WAG and EAG. Meanwhile, the intensified filaments cool the surface at this time of the year and reduce these seasonal amplitudes in the area between both gyres. The seasonality of the Northern Current meridionally separates the eastern Iberian coastal transitional area at Cape of Nao: the northernmost part, fed with cool, salty and remineralized MW during the cold season and influenced by the northward spreading of MAW during the warm season, show the largest seasonal amplitudes for SST, $fCO_{2,sw}$, pH and C_T compared to the southernmost part, supplied with recent MAW during most of the year and by a weak and relatively warmed branch of the Northern Current during winter.

Even with the limitations of five-year observational period, the interannual trends report the relevant acceleration in warming in comparison with the previous two decades (78-88%). The SST increased at rates ranging between 0.26 and 0.43 ºC yr^{-1} and drove a rapid increase in $fCO_{2,sw}$ within 4.18 and 5.53 µatm yr^{-1} and a decrease in pH within -0.0049 and -0.0065 units yr^{-1}. The strengthening of interannual variations during the study period was primarily conducted by the reinforcement of trends, within one-third to one-half, during the warm season in comparison to the cold season. The NC_T decreased at a rate between -0.5 and -1.6 µmol kg^{-1}, suggesting an interannual dismiss in the remineralization/biological production ratio. These progressively variations were counterbalanced along the Eastern Iberian margin by the increasingly relevance of lateral/vertical advection and mesoscale structures, which favours the inflow of remineralized waters mainly during the cold season.

The variations in $fCO_{2,sw}$ were found to be strongly controlled by temperature fluctuations. On a seasonal scale, the rapidly warmed AJ as enters the Alboran Sea drives a significant eastward increase in $dfCO_{2,T}$ compared to $dfCO_{2,NT}$. Consequently, the thermal-driven seasonal changes intensified and doubled those non-thermal as MAW formed, advanced northward along the eastern Iberian margin and mixed with MW. The driver analysis has identified the SST as the primary driver of the seasonality of $fCO_{2,sw}$, accounting for 45-83% of its variations. The processes controlling the C_T offsets 25-38% of the seasonal amplitude of $fCO_{2,sw}$ expected by the effect of thermal-processes. The seasonal variations in A_T infers minor changes in $fCO_{2,sw}$ (<15%) while the contribution

https://doi.org/10.5194/egusphere-2024-2709
Preprint. Discussion started: 7 October 2024
© Author(s) 2024. CC BY 4.0 License.

of SSS fluctuations was close to negligible (<3.5%). The seasonal amplitude of $fCO_{2,sw}$ increased during the study period in the Alboran Sea, while high mesoscale variability along the Eastern Iberian margin infers higher ranges of uncertainties and do not allow to obtain relevant conclusions. Based on the driver analysis, this variation was driven, in first term, by the increasing contribution of temperature (due to the seasonal amplitude of SST is becoming larger) and, in second term, by the decreasing contribution of C_T (due to the dismissing remineralization/production ratio). On an interannual scale, the ~76-92% of the increase in $fCO_{2,sw}$ was described by warming. In the Alboran Sea and extending northward to Cape of Palos, non-thermal processes, primarily biological drawdown during spring blooms, compensated for up to one-third of the expected increase in $fCO_{2,sw}$ due to rising SST. The opposite occurred north of Cape of Palos, where non-thermal processes, mainly the inflow of CO_2-rich MW during the cold season, accounted for the increase in $fCO_{2,sw}$.

The assessment of the air-sea CO_2 exchange shows the Western boundary of the Mediterranean basin undersaturated and acting as a significant sink for atmospheric CO_2 during most of the year, while presented supersaturated conditions which led a CO_2 source status during the warm months. On an annual basis, the entire monitored area acted as a net CO_2 sink. The evolution of the FCO_2 has shown a reduction in the net annual CO_2 invasion at statistically significant rates ranging between 0.06 and 0.13 mol m^{-2} yr^{-1} yr^{-1} (40-80% since 2019), which would reverse the behaviour of the area to a net annual CO_2 source before 2030 if the climate conditions continues the nowadays trends. The weakening in the net annual CO_2 sink was driven by the ongoing strength of the summer outgassing (mainly in the Alboran Sea) and the weakening in the autumn and spring ingassing (throughout the region). Integrating the annual cycle of FCO_2 during the entire study period, net CO_2 ingassing calculated for the Alboran Sea and Eastern Iberian Margin was -1.57 ± 0.49 and -0.70 ± 0.54 mol m^{-2} yr^{-1}.

The present investigation has addressed the need to design and implement systematic observation strategies for characterizing the physico-chemical seawater properties in the Mediterranean basin, an effort that has been required by the scientific community for the last decades. This research pretended to emphasize the efficiency of VOS in the monitoring of the surface physical and MCS variables, particularly in areas subject to high variability under anthropogenic pressure as coastal regions and semi-enclosed seas, where the implementation of other observation-based alternatives is challenging. The

https://doi.org/10.5194/egusphere-2024-2709
Preprint. Discussion started: 7 October 2024
© Author(s) 2024. CC BY 4.0 License.

results improve the comprehension of the MSC dynamics along a coastal transitional area in the Western Mediterranean Sea, which is of high environmental and socio-economic importance and significantly influences the European climate. Likewise, they contribute to a more accurate understanding of the role of coastal areas in the context of Global Change at both basin and global scales. Although the study period was relatively short and larger time-series are necessary for quantifying long-term trends and making future projections, it has encompassed drastic variations compared to previous decades likely caused by isolated events feedbacked by climate change (i. e. marine heat waves). This has enabled the study of physicochemical dynamics under conditions expected for the future state of the ocean.

Code Availability

The $CO_{2,SYS}$ programme for MATLAB is available at https://github.com/jonathansharp/CO2-System-Extd.

Data Availability Statement

The underway observations provided by the SOOP CanOA-VOS in the Western Mediterranean Sea (February 2019 – February 2024) used in this investigation are published in open-access at Zenodo (doi.org/10.5281/zenodo.13379011) and available in since September 2023 at the ICOS Data Portal (https://www.icos-cp.eu/data-products/ocean-release). The SST reanalysis monthly data (0.042º x 0.042º) from the Med MFC physical multiyear product (Escudier et al., 2020; 2021; Nigam et al., 2021) are available at Copernicus Marine Data Store (https://data.marine.copernicus.eu/products). ERA5 hourly wind speed reanalysis data at 10 m above the sea level used to calculate air-sea CO_2 fluxes is available at Copernicus Climate Data Store (https://cds.climate.copernicus.eu/).

Author contribution

All the authors made significant contributions on this research. M. G.-D., J. M. S.-C. and A.G.G. installed and maintained the equipment in the VOS. D. C-H and D. G-S participated in routine maintenance and data acquisition. D. C.-H. developed the MATLAB® routines and conducted the data processing and analysis. All authors contributed to the writing of the manuscript and supported its submission.

https://doi.org/10.5194/egusphere-2024-2709
Preprint. Discussion started: 7 October 2024
© Author(s) 2024. CC BY 4.0 License.

Declaration Competing interest

The authors declare that the research was conducted in the absence of any commercial or financial relationships that could be construed as a potential conflict of interest.

Acknowledgement

This research was supported by the Canary Islands Government and the Loro Parque Foundation through the CanBIO project, CanOA subproject (2019–2024), and the CARBOCAN agreement (Consejería de Transición Ecológica y Energía, Gobierno de Canarias). We would like to thank the JONA SOPHIE ship owner, Reederei Stefan Patjens GmbH & Co. KG, the NISA-Marítima company and the captains and crew members for the support during this collaboration. Special thanks to the technician Adrian Castro-Álamo for biweekly equipment maintenance and discrete sampling of total alkalinity aboard the ship. The SOOP CanOA-VOS line is part of the Spanish contribution to the Integrated Carbon Observation System (ICOS-ERIC; https://www.icos-cp.eu/) since 2021 and has been recognized as an ICOS Class 1 Ocean Station. The participation of D. C-H was funded by the PhD grant PIFULPGC-2020-2 ARTHUM-2

https://doi.org/10.5194/egusphere-2024-2709
Preprint. Discussion started: 7 October 2024
© Author(s) 2024. CC BY 4.0 License.

Legend for Figures

Figure 1. (a) Map of the Western boundary of the Mediterranean Sea with the CanOA-VOS tracks between February 2019 and February 2024 (red) and the location of the stations of interest along the southern (S1-S5) and eastern (E1-E6) sections. The main Capes and Gulf along the geographically rugged Iberian coastline are shown. The schematic diagram summarized the classical circulation patterns: in the Alboran Sea (blue), the Atlantic Jet (AJ) surrounds the Western and Eastern Anticyclonic Gyres (WAG and EAG, respectively) and forms Modified Atlantic Water (MAW), while along the Eastern Iberian margin (purple), the Mediterranean Water (MW) is transported from the Northwestern Mediterranean basin along the path of the Northern Current. The northward spreading of MAW during summer and southward spreading MW during winter is depicted with dashed arrows. The thermal front formed in the axis of the Pyrenees during summer is depicted with a black dashed line. (b) SST maps built with reanalysis monthly data (0.042º x 0.042º) for February and September 2023 from the Med MFC physical multiyear product (Escudier et al., 2020; 2021; Nigam et al., 2021), available at Copernicus Marine Data Store (https://data.marine.copernicus.eu/products).

Figure 2. Spatial distribution of the average SST, $fCO_{2,sw}$, pH, and C_T calculated on a seasonal and annual basis every 0.1º longitude along the S section (left panels) and every 0.25º latitude along the E section (right panels). The 3-months periods January-March, April-June, July-September and October-December were considered as winter, spring, summer and autumn, respectively. Note the different scales used for C_T due to significant variations between the S and E sections. Standard deviations are provided in Table Sup1 and indicate the range of variability among the study period.

Figure 3. Time-series of SST, $fCO_{2,sw}$ and pH at S1, S3 and S5 along the eastern Iberian margin within the five years of observations. The weekly average data was fitted to harmonic Eq. 10. The thermal and non-thermal terms of the average $fCO_{2,sw}$ calculated by following the procedures of Takahashi et al., 2002 (T,02) and Fassbender et al., 2022 (F'22) and the pH_{19} are depicted. The coefficients *a-f*, standard errors of estimate and r^2 given by Eq. 10 are presented in Table Sup1.

Figure 4. Time-series of SST, $fCO_{2,sw}$ and pH at E1, E4 and E5 in the Alboran Sea within the five years of observations. The weekly average data was fitted to harmonic Eq. 10. The thermal and non-thermal terms of the average $fCO_{2,sw}$ calculated by following the

https://doi.org/10.5194/egusphere-2024-2709
Preprint. Discussion started: 7 October 2024
© Author(s) 2024. CC BY 4.0 License.

procedures of Takahashi et al., 2002 (T,02) and Fassbender et al., 2022 (F'22) and the pH_{19} are depicted. The coefficients *a-f*, standard errors of estimate and r^2 given by Eq. 10 are presented in Table Sup1.

Figure 5. Temporal evolution of the seasonal rates of $fCO_{2,sw}$ explained by each of its drivers within the five years of observation. The differences between monthly average data for February and September (where minimum and maximum SST and $fCO_{2,sw}$ were encountered) was considered to compute the seasonal trends. The standard deviation of the monthly average data were considered in the calculation of the seasonal changes and infers errors in the computation of $fCO_{2,sw}$, which are summarized in Table Sup3. The cumulative $fCO_{2,sw}$ change resulting from the distinct impulsors $\frac{dfCO_{2,sw}}{dt}$ (sum) were consistent with the observed seasonal ΔfCO_2 trends ($\frac{dfCO_{2,sw}}{dt}$ (obs)), thereby instilling confidence in the methodology.

Figure 6. Temporal variations of CO_2f (blue; left axis), ΔfCO_2 (orange; right axis) and wind speed (gray; left axis) at (a) S1-S5 and (b) E1-E6. A piecewise polynomial-based smoothing spline was applied to the weekly average data (represented with dots). Gaps were covered by the harmonic fitting (Eq. 10; dash line). The black lines represent the interannual increase in CO_2f. The seasonally-detrended interannual rates of change of CO_2f and ΔfCO_2 are shown in each panel. *** denotes that the trends are statistically significant at the 99% level of confidence, ** at the 95% level of confidence and * at the 90% level of confidence. The wind speed does not show statistically significant interannual trends (p-values > 0.1).

Figure 7. Temporal evolution of average CO_2f calculated on a seasonal and annual basis for each year (2019-2023) at S1-S5 and E1-E6. Same representation for ΔfCO_2 and wind speed is available in Figure Sup5 and Sup6. The 3-months periods January-March, April-June, July-September and October-December were considered as winter, spring, summer and autumn, respectively. The legend includes the interannual trends for CO_2f (mol m^{-2} yr^{-1}) based on linear regression of the seasonal and annual means. *** denotes that the trends are statistically significant at the 99% level of confidence, ** at the 95% level of confidence and * at the 90% level of confidence. Standard deviations are presented in Table Sup4.

Legend for Tables

https://doi.org/10.5194/egusphere-2024-2709
Preprint. Discussion started: 7 October 2024
© Author(s) 2024. CC BY 4.0 License.

Table 1. Seasonal amplitudes and interannual trends of SST, SSS, $fCO_{2,sw}$, pH, pH_{19}, C_T and NC_T. The seasonal changes were calculated as the amplitude of Eq. 10 fitted to the weekly average data at each station. The error of the seasonal amplitudes was assumed as the product of the standard error of estimate given by the harmonic function by 2. The interannual changes were based on linear regressions and given for each station and for the entire S and E sections (considering the total amount of average data at S1-S5 and E1-E6, respectively) during the cold and warm season. The interannual trends of SST during 2000-2019 (based on reanalysis monthly data from the Med MFC physical multiyear product [Escudier et al., 2020; 2021; Nigam et al., 2021]; detailed in section 4.2) was included for comparison. The trends were obtained by the linear regressions of the seasonally-detrended weekly average data and include their standard error of estimate. *** denotes that the trends are statistically significant at the 99% level of confidence, ** at the 95% level of confidence and * at the 90% level of confidence.

Table 2. Means, seasonal amplitudes and interannual rates of change of thermal and non-thermal components of $fCO_{2,sw}$ ($fCO_{2,T}$ and $fCO_{2,NT}$, respectively) calculated by following Takahashi et al., 2002 and Fassbender et al., 2022 (T'02 and T'22, respectively). The seasonal changes were calculated as the amplitude of Eq. 10 fitted to the weekly average data at each station. The error of the seasonal amplitudes was assumed as twice the standard error of estimate given by the harmonic function. The trends were obtained by the linear regressions of the seasonally-detrended weekly average data and include their standard error of estimate. *** denotes that the trends are statistically significant at the 99% level of confidence, ** at the 95% level of confidence and * at the 90% level of confidence.

https://doi.org/10.5194/egusphere-2024-2709
Preprint. Discussion started: 7 October 2024
© Author(s) 2024. CC BY 4.0 License.

1070 Fig. 1

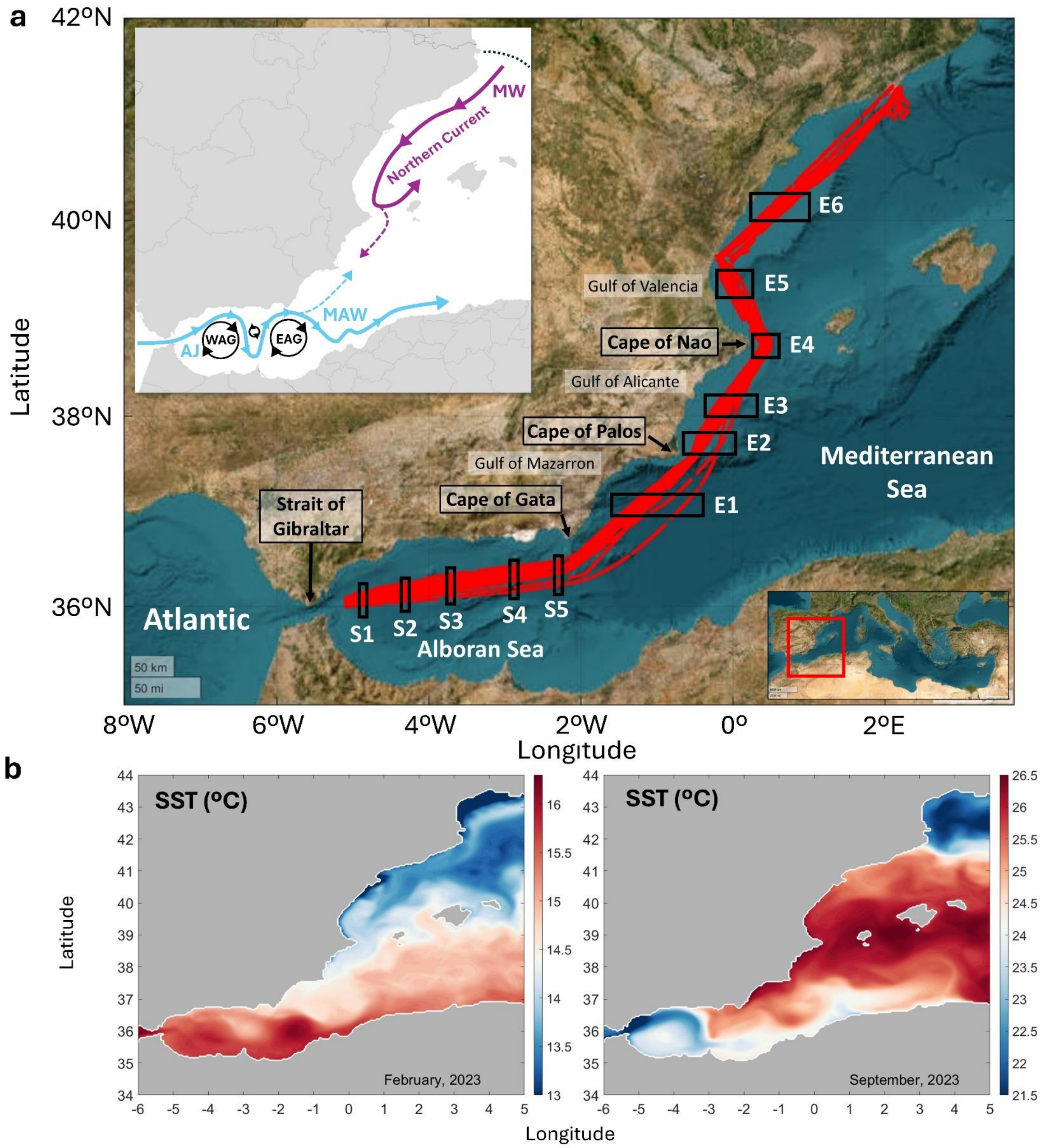

https://doi.org/10.5194/egusphere-2024-2709
Preprint. Discussion started: 7 October 2024
© Author(s) 2024. CC BY 4.0 License.

1071 Fig. 2

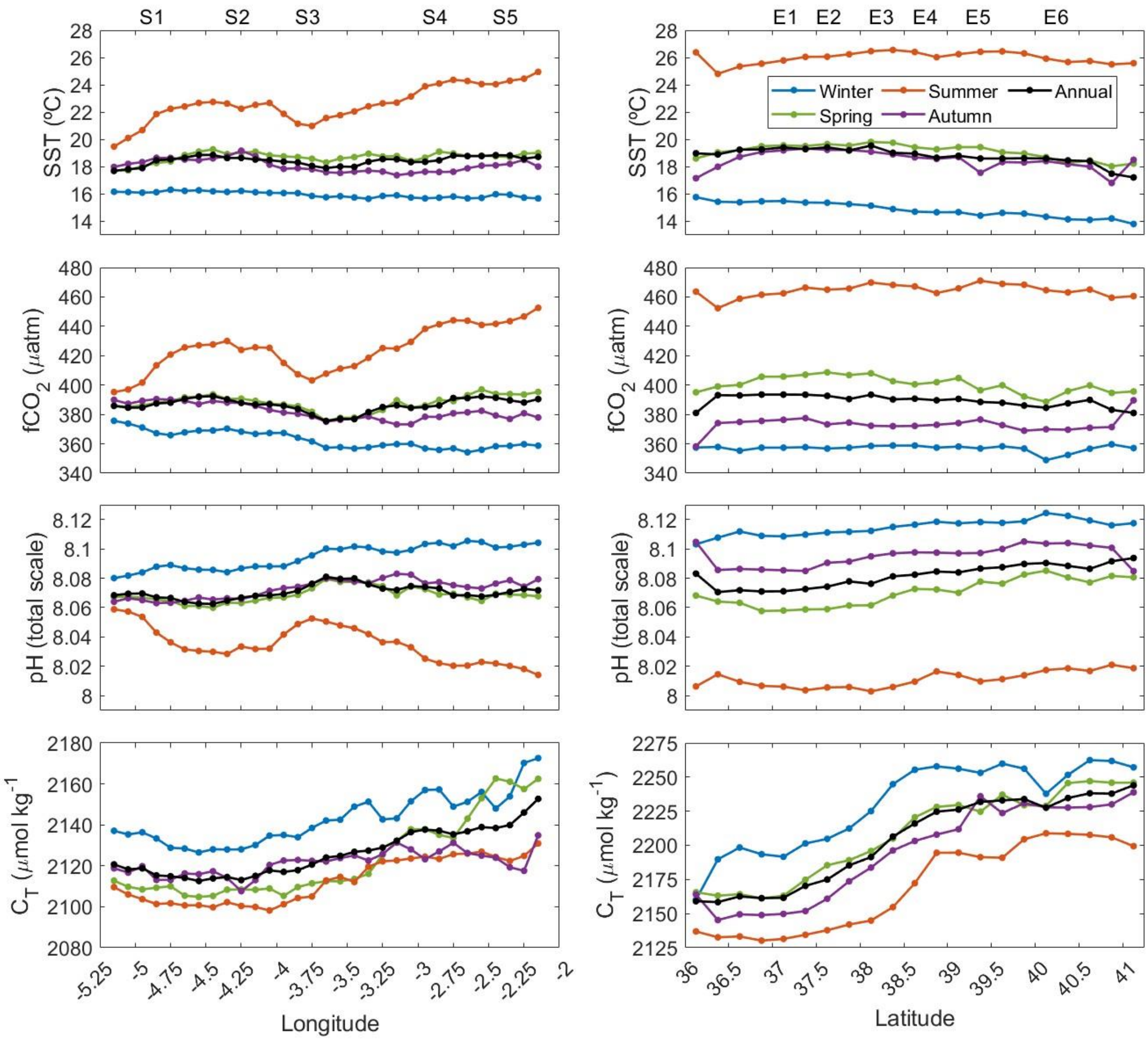

https://doi.org/10.5194/egusphere-2024-2709
Preprint. Discussion started: 7 October 2024
© Author(s) 2024. CC BY 4.0 License.

1072 Fig. 3

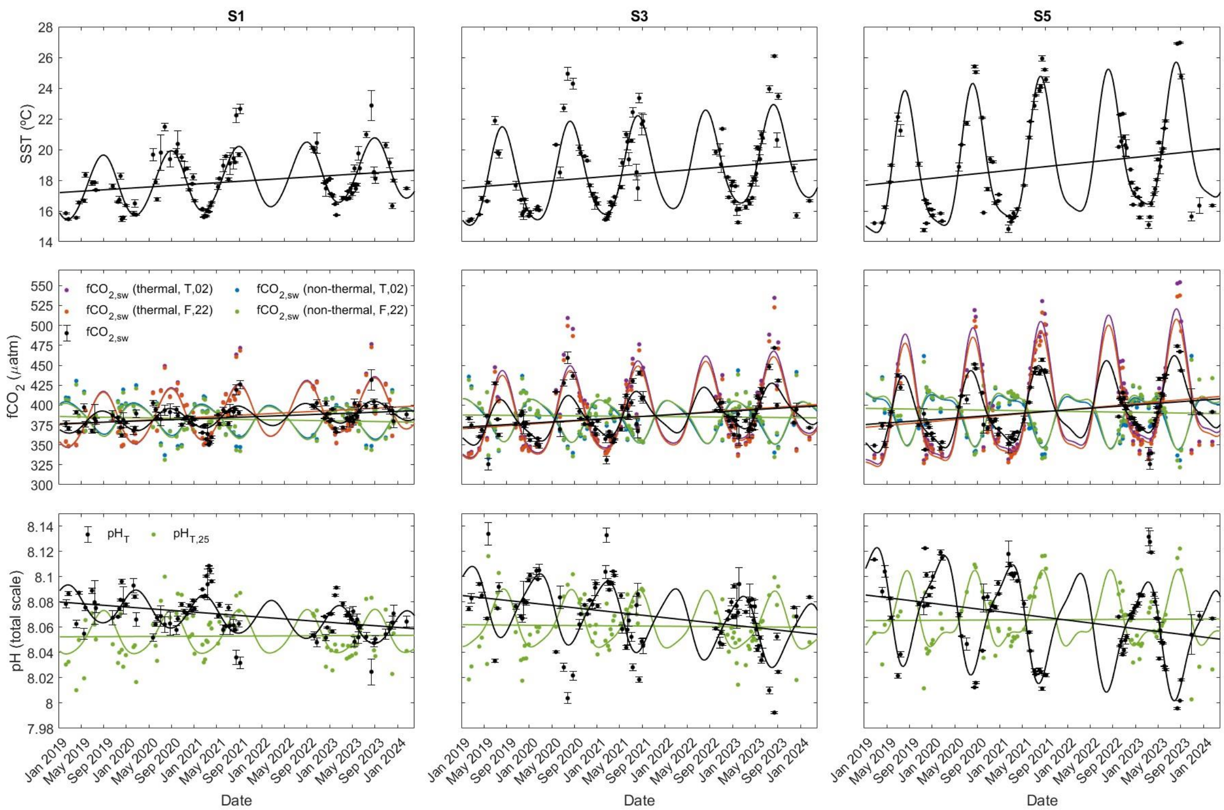

https://doi.org/10.5194/egusphere-2024-2709
Preprint. Discussion started: 7 October 2024
© Author(s) 2024. CC BY 4.0 License.

1073 Fig. 4

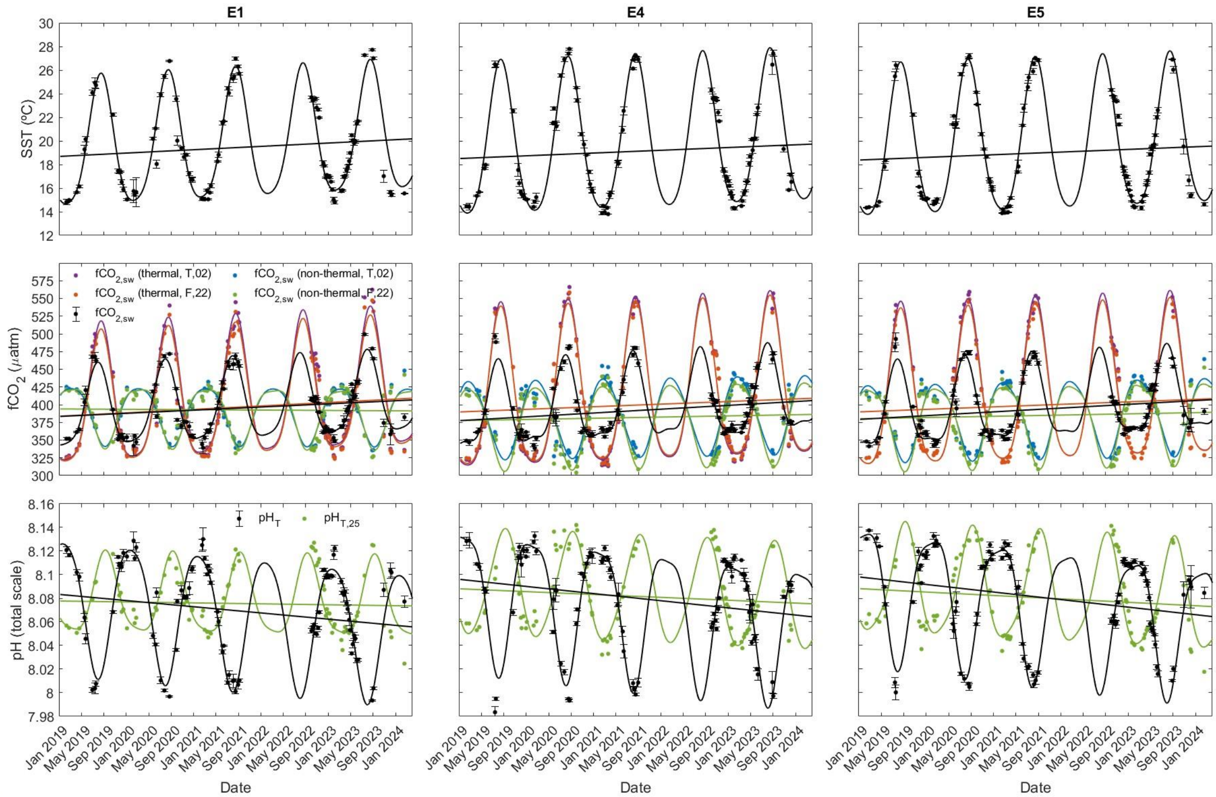

https://doi.org/10.5194/egusphere-2024-2709
Preprint. Discussion started: 7 October 2024
© Author(s) 2024. CC BY 4.0 License.

1074 Fig. 5

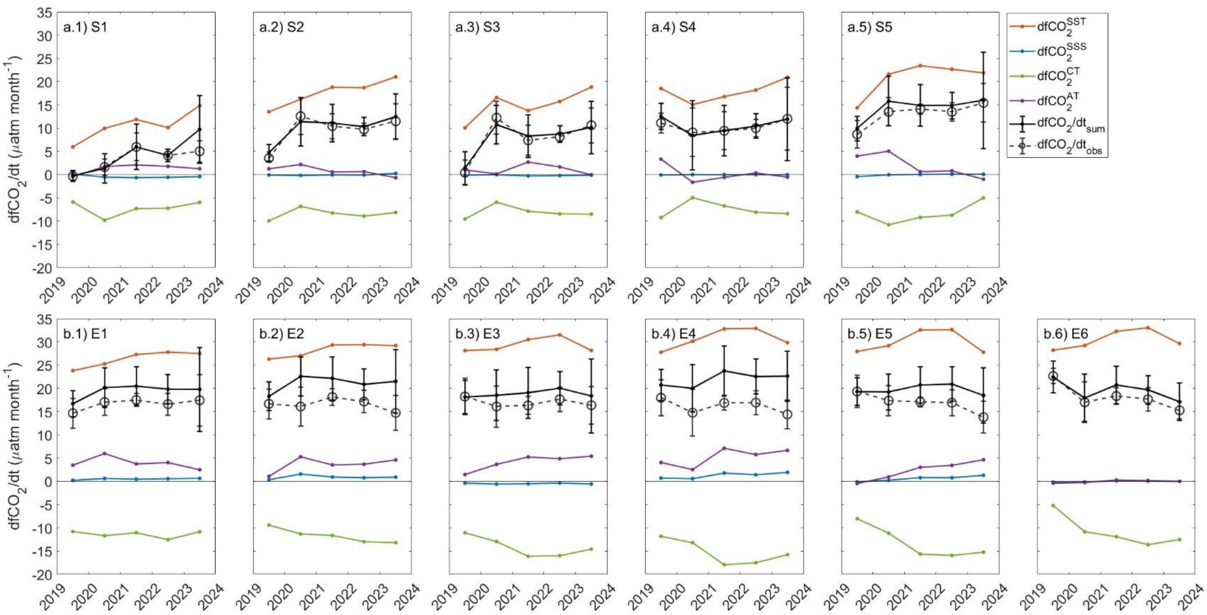

https://doi.org/10.5194/egusphere-2024-2709
Preprint. Discussion started: 7 October 2024
© Author(s) 2024. CC BY 4.0 License.

Fig. 6

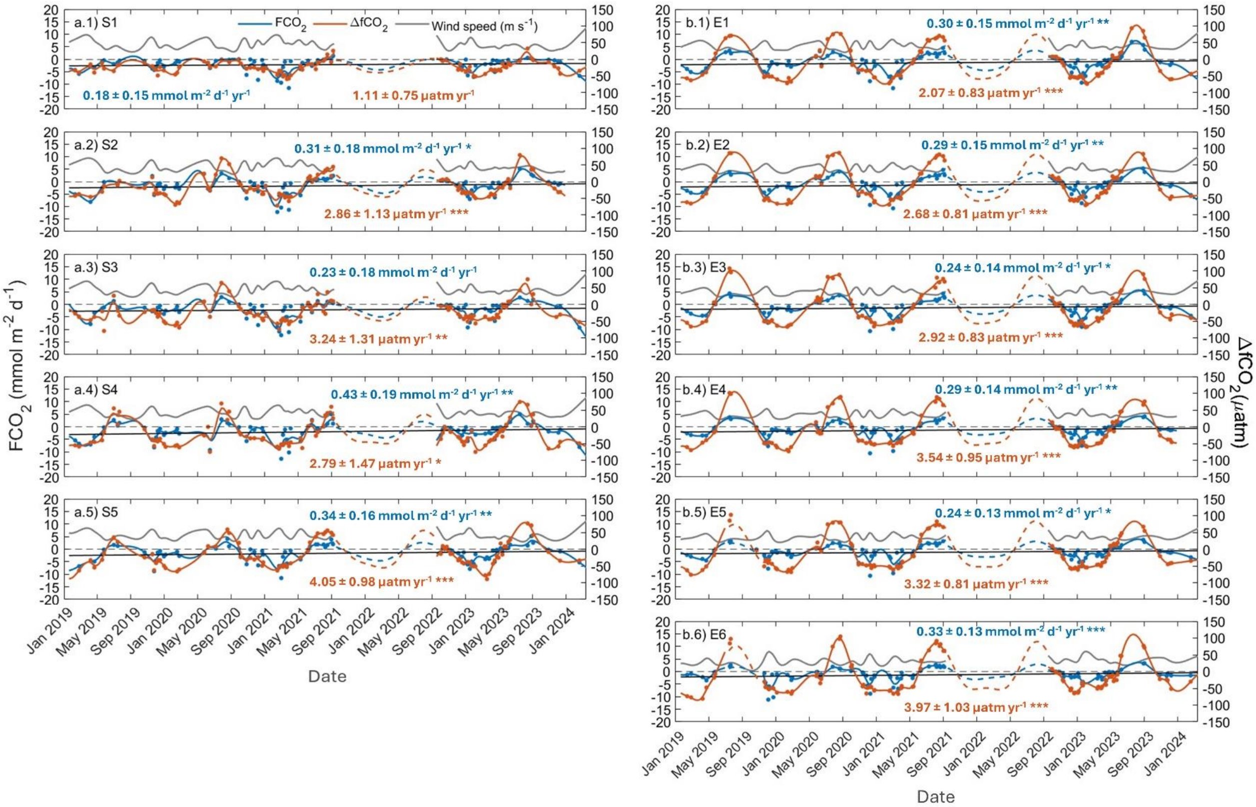

https://doi.org/10.5194/egusphere-2024-2709
Preprint. Discussion started: 7 October 2024
© Author(s) 2024. CC BY 4.0 License.

Fig. 7

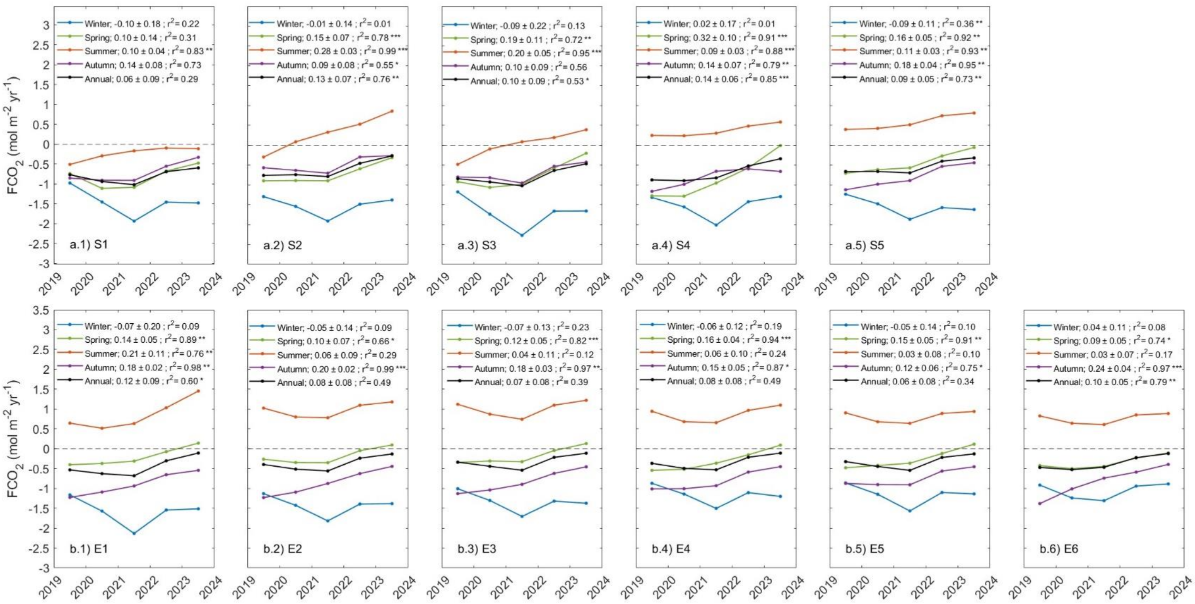

© Author(s) 2024. CC BY 4.0 License.

Table 1

Hoja de cálculo de Microsoft Excel

	SST		SSS		$fCO_{2,sw}$		pH		pH_{19}		C_T		NC_T		A_T		NA_T	
	Seasonal amplitude (ºC)	ratio (ºC yr^{-1})	Seasonal amplitude	ratio (yr^{-1})	Seasonal amplitude (μatm)	ratio (μatm yr^{-1})	Seasonal amplitude (total scale)	ratio (units yr^{-1})	Seasonal amplitude (total scale)	ratio (units yr^{-1})	Seasonal amplitude (μmol kg^{-1})	ratio (μmol kg^{-1} yr^{-1})	Seasonal amplitude (μmol kg^{-1})	ratio (μmol kg^{-1} yr^{-1})	Seasonal amplitude (μmol kg^{-1})	ratio (μmol kg^{-1} yr^{-1})	Seasonal amplitude (μmol kg^{-1})	ratio (μmol kg^{-1} yr^{-1})
S1	4.21 ± 1.90	0.28 ± 0.07 ***	0.293 ± 0.328	-0.074 ± 0.012 ***	27.78 ± 20.27	3.13 ± 0.75 ***	0.0300 ± 0.0210	-0.0040 ± 0.0008 ***	0.0344 ± 0.0280	0.0002 ± 0.0010	41.2 ± 16.3	-6.4 ± 1.0 ***	26.8 ± 16.3	-2.2 ± 0.6 ***	29.4 ± 32.8	-7.4 ± 1.2 ***	10.6 ± 5.9	-2.7 ± 0.4 ***
S2	7.50 ± 2.18	0.50 ± 0.09 ***	0.158 ± 0.258	-0.078 ± 0.010 ***	70.20 ± 28.27	4.68 ± 1.10 ***	0.0674 ± 0.0254	-0.0055 ± 0.0010 ***	0.0582 ± 0.0292	0.0022 ± 0.0011 *	37.3 ± 19.4	-7.9 ± 1.1 ***	35.4 ± 19.4	-3.5 ± 0.8 ***	15.6 ± 25.9	-7.9 ± 1.0 ***	5.6 ± 4.7	-2.9 ± 0.4 ***
S3	6.42 ± 2.38	0.36 ± 0.09 ***	0.333 ± 0.334	-0.070 ± 0.012 ***	57.23 ± 35.36	5.12 ± 1.32 ***	0.0563 ± 0.0340	-0.0059 ± 0.0013 ***	0.0455 ± 0.0276	-0.0004 ± 0.0010	47.4 ± 17.6	-5.7 ± 1.1 ***	33.0 ± 17.6	-1.8 ± 0.7 ***	33.4 ± 33.7	-7.0 ± 1.3 ***	12.1 ± 6.1	-2.6 ± 0.5 ***
S4	7.53 ± 2.58	0.26 ± 0.10 ***	0.344 ± 0.457	-0.051 ± 0.017 ***	74.89 ± 38.91	4.89 ± 1.45 ***	0.0698 ± 0.0372	-0.0053 ± 0.0014 ***	0.0544 ± 0.0242	-0.0014 ± 0.0009	43.0 ± 19.9	-3.6 ± 1.6 ***	33.0 ± 19.9	-0.6 ± 0.7	34.7 ± 46.3	-5.2 ± 1.7 ***	12.5 ± 8.2	-1.9 ± 0.6 ***
S5	9.25 ± 2.34	0.45 ± 0.09 ***	0.562 ± 0.575	-0.062 ± 0.022 ***	96.99 ± 25.18	6.17 ± 0.98 ***	0.0940 ± 0.0242	-0.0067 ± 0.0009 ***	0.0601 ± 0.0304	0.0003 ± 0.0012	50.8 ± 24.3	-5.6 ± 2.0 ***	34.3 ± 24.3	-2.0 ± 0.9 ***	56.6 ± 58.0	-6.3 ± 2.2 ***	20.1 ± 10.3	-2.3 ± 0.8 ***
summer		0.59 ± 0.20 ***		-0.031 ± 0.021		7.23 ± 2.33 ***		-0.0069 ± 0.0020 ***		0.0020 ± 0.0014		-3.9 ± 1.4 ***		-2.1 ± 0.7 ***		-3.1 ± 2.2		-1.1 ± 0.8
winter		0.26 ± 0.04 ***		-0.094 ± 0.020 ***		3.43 ± 0.96 ***		-0.0047 ± 0.0011 ***		-0.0006 ± 0.0010		-7.8 ± 1.8 ***		-2.4 ± 0.8 ***		-9.5 ± 2.0 ***		-3.4 ± 0.7 ***
total		0.38 ± 0.05 ***		-0.065 ± 0.009 ***		4.76 ± 0.59 ***		-0.0054 ± 0.0006 ***		0.0002 ± 0.0005		-5.7 ± 0.8 ***		-2.0 ± 0.4 ***		-6.6 ± 0.9 ***		-2.4 ± 0.3 ***
2000-2019		0.03 ± 0.00 ***																
E1	11.07 ± 2.15	0.28 ± 0.08 ***	0.522 ± 0.463	-0.069 ± 0.017 ***	116.94 ± 23.18	4.44 ± 0.85 ***	0.1148 ± 0.0234	-0.0052 ± 0.0009 ***	0.0670 ± 0.0206	-0.0008 ± 0.0008	81.1 ± 15.1	-5.5 ± 1.4 ***	52.6 ± 15.1	-1.5 ± 0.6 ***	52.7 ± 47.0	-7.0 ± 1.7 ***	18.3 ± 8.2	-2.4 ± 0.6 ***
E2	11.64 ± 1.82	0.31 ± 0.07 ***	0.482 ± 0.486	-0.094 ± 0.018 ***	121.57 ± 21.54	4.79 ± 0.81 ***	0.1172 ± 0.0218	-0.0059 ± 0.0008 ***	0.0732 ± 0.0190	-0.0011 ± 0.0007	83.2 ± 13.5	-7.4 ± 1.5 ***	56.8 ± 13.5	-1.9 ± 0.5 ***	48.8 ± 49.2	-9.5 ± 1.9 ***	16.9 ± 8.5	-3.3 ± 0.6 ***
E3	12.44 ± 1.89	0.24 ± 0.07 ***	0.592 ± 0.604	-0.138 ± 0.023 ***	124.78 ± 21.85	4.99 ± 0.82 ***	0.1225 ± 0.0204	-0.0067 ± 0.0008 ***	0.0818 ± 0.0236	-0.0031 ± 0.0009 ***	94.1 ± 21.4	-10.2 ± 2.0 ***	63.9 ± 21.4	-2.0 ± 0.8 ***	60.0 ± 61.2	-14.0 ± 2.3 ***	20.6 ± 10.5	-4.8 ± 0.8 ***
E4	13.04 ± 1.80	0.23 ± 0.07 ***	0.768 ± 0.493	-0.068 ± 0.018 ***	120.73 ± 25.43	5.40 ± 0.94 ***	0.1196 ± 0.0234	-0.0061 ± 0.0009 ***	0.0891 ± 0.0280	-0.0024 ± 0.0010 **	120.1 ± 21.6	-4.4 ± 1.7 ***	75.1 ± 21.6	-0.4 ± 0.8	77.9 ± 49.9	-6.9 ± 1.8 ***	26.5 ± 8.5	-2.3 ± 0.6 ***
E5	12.92 ± 1.74	0.23 ± 0.06 ***	0.538 ± 0.467	-0.097 ± 0.017 ***	118.88 ± 21.72	5.31 ± 0.79 ***	0.1165 ± 0.0194	-0.0064 ± 0.0007 ***	0.0914 ± 0.0270	-0.0029 ± 0.0010 ***	98.4 ± 20.8	-6.6 ± 1.6 ***	69.3 ± 20.8	-0.9 ± 0.7	54.6 ± 47.3	-9.9 ± 1.7 ***	18.5 ± 8.0	-3.3 ± 0.6 ***
E6	13.13 ± 2.02	0.19 ± 0.07 ***	0.108 ± 0.551	-0.011 ± 0.015	124.68 ± 30.17	6.09 ± 0.99 ***	0.1159 ± 0.0256	-0.0061 ± 0.0008 ***	0.0929 ± 0.0328	-0.0032 ± 0.0011 ***	63.3 ± 27.4	0.9 ± 1.6	59.3 ± 27.4	1.6 ± 0.9	10.0 ± 54.7	-1.2 ± 1.4	3.4 ± 9.2	-0.4 ± 0.5
summer		0.29 ± 0.09 ***		-0.069 ± 0.042 *		-2.30 ± 1.02 **		0.0011 ± 0.0008		0.0037 ± 0.0012 ***		-8.5 ± 3.2 ***		-4.3 ± 0.9 ***	±	-7.0 ± 4.3	±	-2.4 ± 1.5
winter		0.20 ± 0.04 ***		-0.092 ± 0.023 ***		5.44 ± 0.41 ***		-0.0067 ± 0.0005 ***		-0.0036 ± 0.0007 ***		-5.8 ± 2.1 ***		-0.4 ± 0.8	±	-9.4 ± 2.4 ***	±	-3.2 ± 0.8 ***
total		0.30 ± 0.04 ***		-0.082 ± 0.013 ***		5.16 ± 0.37 ***		-0.0061 ± 0.0004 ***		-0.0022 ± 0.0004 ***		-5.8 ± 1.1 ***		-0.9 ± 0.4 ***	±	-8.4 ± 1.3 ***	±	-2.9 ± 0.4 ***
2000-2019		0.05 ± 0.01 ***																

https://doi.org/10.5194/egusphere-2024-2709
Preprint. Discussion started: 7 October 2024
© Author(s) 2024. CC BY 4.0 License.

Table 2

	$fCO_{2,sw}$ (thermal)						$fCO_{2,sw}$ (non-thermal)						T/B ratio	
	T'02			F'22			T'02			F'22				
	Mean (µatm)	Seasonal Amplitude (µatm)	Interannual ratio (µatm yr⁻¹)	Mean (µatm)	Seasonal Amplitude (µatm)	Interannual ratio (µatm yr⁻¹)	Mean (µatm)	Seasonal Amplitude (µatm)	Interannual ratio (µatm yr⁻¹)	Mean (µatm)	Seasonal Amplitude (µatm)	Interannual ratio (µatm yr⁻¹)	T'02	F'22
S1		70.35 ± 16.39	4.53 ± 1.21 ***		68.40 ± 15.85	4.42 ± 1.17 ***		41.04 ± 14.67	-1.53 ± 1.08		41.44 ± 14.70	-1.35 ± 1.09	1.71	1.65
S2		129.76 ± 19.66	8.50 ± 1.53 ***		124.45 ± 18.69	8.18 ± 1.46 ***		66.85 ± 17.44	-3.83 ± 1.36 ***		67.53 ± 15.90	-3.50 ± 1.24 ***	1.94	1.84
S3	392.04 ± 40.87	109.35 ± 21.50	6.04 ± 1.60 ***	389.02 ± 39.15	104.93 ± 20.41	5.80 ± 1.52 ***	386.13 ± 18.44	54.11 ± 15.14	-0.79 ± 1.13	386.62 ± 18.77	54.02 ± 14.31	-0.68 ± 1.06	2.02	1.94
S4		131.09 ± 23.60	4.36 ± 1.76 **		125.63 ± 22.41	4.19 ± 1.67 ***		59.99 ± 14.14	0.82 ± 1.05		61.82 ± 13.68	0.74 ± 1.02	2.19	2.03
S5		163.37 ± 20.70	7.79 ± 1.61 ***		154.95 ± 19.60	7.43 ± 1.52 ***		65.16 ± 17.94	-1.31 ± 1.39		68.85 ± 16.76	-1.25 ± 1.30	2.51	2.25
summer			11.83 ± 3.68 ***			11.09 ± 3.39 ***			-2.92 ± 1.23 **			-3.94 ± 1.44 ***		
winter			3.97 ± 0.70 ***			3.81 ± 0.74 ***			-0.62 ± 1.16			-0.29 ± 1.03		
total			6.20 ± 0.81 ***			5.94 ± 0.77 ***			-1.27 ± 0.57 **			-1.14 ± 0.55 **		
E1		196.07 ± 19.09	5.11 ± 1.40 ***		186.41 ± 18.12	4.84 ± 1.32 ***		81.74 ± 10.92	-0.18 ± 0.80		83.96 ± 10.83	-0.53 ± 0.79	2.40	2.22
E2		206.32 ± 16.29	5.29 ± 1.23 ***		196.92 ± 15.51	5.09 ± 1.17 ***		89.84 ± 9.73	-0.07 ± 0.73		91.97 ± 9.61	-0.32 ± 0.72	2.30	2.14
E3	400.22 ± 70.68	219.12 ± 16.15	3.86 ± 1.20 ***	399.02 ± 67.76	213.60 ± 15.79	3.80 ± 1.17 ***	389.61 ± 32.15	99.59 ± 13.95	1.43 ± 1.03	385.00 ± 33.52	105.81 ± 13.10	1.21 ± 0.97	2.20	2.02
E4		230.66 ± 15.37	3.75 ± 1.13 ***		222.49 ± 14.90	3.68 ± 1.10 ***		110.60 ± 15.39	1.58 ± 1.13		116.16 ± 15.56	1.67 ± 1.15	2.09	1.92
E5		229.35 ± 14.52	3.64 ± 1.05 ***		219.99 ± 14.06	3.55 ± 1.01 ***		108.60 ± 15.35	1.93 ± 1.11 *		115.03 ± 14.74	1.72 ± 1.06	2.11	1.91
E6		231.16 ± 17.30	2.88 ± 1.28 **		221.64 ± 16.61	2.84 ± 1.23 **		104.92 ± 19.24	3.37 ± 1.33 ***		109.10 ± 18.90	3.25 ± 1.29 ***	2.20	2.03
summer			6.41 2.13 ***			5.85 2.07 ***			-4.79 1.12 ***			-6.62 1.63 ***		
winter			2.78 0.60 ***			2.77 0.59 ***			2.91 0.83 ***			2.62 0.67 ***		
total			4.10 0.52 ***			3.95 0.51 ***			1.33 0.46 ***			1.19 0.47 ***		

https://doi.org/10.5194/egusphere-2024-2709
Preprint. Discussion started: 7 October 2024
© Author(s) 2024. CC BY 4.0 License.

References

Alberola, C., Millot, C., and Font, J.: On the seasonal and mesoscale variabilities of the Northern Current during the PRIMO-0 experiment in the western Mediterranean Sea, Oceanol. Acta, 18, 163–192, 1995.

Álvarez, M., Sanleón-Bartolomé, H., Tanhua, T., Mintrop, L., Luchetta, A., Cantoni, C., Schroeder, K., and Civitarese, G.: The CO2 system in the Mediterranean Sea: a basin-wide perspective, Ocean Sci., 10, 69–92, https://doi.org/10.5194/os-10-69-2014, 2014.

Antoine, D., Chami, M., Claustre, H., d'Ortenzio, F., Morel, A., Bécu, G., Gentili, B., Louis, F., Ras, J., Roussier, E., Scott, A. J., Tailliez, D., Hooker, S. B., Guevel, P., Desté, J. F., Dempsey, C., and Adams, D.: BOUSSOLE: A joint CNRS-INSU, ESA, CNES, and NASA ocean color calibration and validation activity, NASA Tech. Memo., 1–59, 2006.

Antoine, D., d'Ortenzio, F., Hooker, S. B., Bécu, G., Gentili, B., and Tailliez, D., Scott, A. J.: Assessment of uncertainty in the ocean reflectance determined by three satellite ocean color sensors (MERIS, SeaWiFS and MODIS-A) at an offshore site in the Mediterranean Sea (BOUSSOLE project), J. Geophys. Res. Ocean., 113, https://doi.org/10.1029/2007JC004472, 2008a.

Antoine, D., Guevel, P., Desté, J. F., Bécu, G., Louis, F., Scott, A. J., and Bardey, P.: The "BOUSSOLE" Buoy - A new transparent-to-swell taut mooring dedicated to marine optics: Design, tests, and performance at sea, J. Atmos. Ocean. Technol., 25, 968–989, https://doi.org/10.1175/2007JTECHO563.1, 2008b.

Bates, N. R., Astor, Y. M., Church, M. J., Currie, K., Dore, J. E., González-Dávila, M., Lorenzoni, L., Muller-Karger, F., Olafsson, J., and Santana-Casiano, J. M.: A time-series view of changing surface ocean chemistry due to ocean uptake of anthropogenic CO2 and ocean acidification, Oceanography, 27, 126–141, https://doi.org/10.5670/oceanog.2014.16, 2014.

Bégovic, M., and Copin-Montégut, C.: Processes controlling annual variations in the partial pressure of CO2 in surface waters of the central northwestern Mediterranean Sea (Dyfamed site), Deep Sea Res. Part II Top. Stud. Oceanogr., 49, 2031–2047, https://doi.org/10.1016/S0967-0645(02)00026-7, 2002.

https://doi.org/10.5194/egusphere-2024-2709
Preprint. Discussion started: 7 October 2024
© Author(s) 2024. CC BY 4.0 License.

Bergamasco, A., and Malanotte-Rizzoli, P.: The circulation of the Mediterranean Sea: a historical review of experimental investigations, Adv. Oceanogr. Limnol., 1, 11–28, https://doi.org/10.1080/19475721.2010.505354, 2010.

Bolado-Penagos, M., González, C. J., Chioua, J., Sala, I., Jesús Gomiz-Pascual, J., Vázquez, Á., and Bruno, M.: Submesoscale processes in the coastal margins of the Strait of Gibraltar. The Trafalgar – Alboran connection, Prog. Oceanogr., 181, 102219, https://doi.org/10.1016/j.pocean.2019.102219, 2020.

Borges, A. V., Delille, B., and Frankignoulle, M.: Budgeting sinks and sources of CO2 in the coastal ocean: Diversity of ecosystem counts, Geophys. Res. Lett., 32, 1–4, https://doi.org/10.1029/2005GL023053, 2005.

Borghini, M. B. H. S., Bryden, H., Schroeder, K., Sparnocchia, S., and Vetrano, A.: The Mediterranean is becoming saltier, Ocean Sci., 10, 693–700, https://doi.org/10.5194/os-10-693-2014, 2014.

Bormans, M., and Garrett, C.: A simple criterion for gyre formation by the surface outflow from a strait, with application to the Alboran Sea, J. Geophys. Res. Ocean., 94, 12,637–12,644, https://doi.org/10.1029/JC094iC09p12637, 1989.

Bosse, A., Testor, P., Damien, P., Estournel, C., Marsaleix, P., Mortier, L., Prieur, L., and Taillandier, V.: Wind-forced submesoscale symmetric instability around deep convection in the northwestern Mediterranean Sea, Fluids, 6, 1–26, https://doi.org/10.3390/fluids6030123, 2021.

Bourg, N., and Molcard, A.: Northern boundary current variability and mesoscale dynamics: a long-term HF RADAR monitoring in the North-Western Mediterranean Sea, Ocean Dyn., 71, 851–870, https://doi.org/10.1007/s10236-021-01466-9, 2021.

Bray, N. A., Ochoa, J., and Kinder, T. H.: The role of the interface in exchange through the Strait of Gibraltar, J. Geophys. Res., https://doi.org/10.1029/95JC00381, 1995.

Cai, W. J., Dai, M., and Wang, Y.: Air-sea exchange of carbon dioxide in ocean margins: A province-based synthesis, Geophys. Res. Lett., 33, https://doi.org/10.1029/2006GL026219, 2006.

https://doi.org/10.5194/egusphere-2024-2709
Preprint. Discussion started: 7 October 2024
© Author(s) 2024. CC BY 4.0 License.

Chen, C. T. A., Huang, T. H., Chen, Y. C., Bai, Y., He, X., and Kang, Y.: Air-sea exchanges of CO2 in the world's coastal seas, Biogeosciences, 10, 6509–6544, https://doi.org/10.5194/bg-10-6509-2013, 2013.

Conan, P., and Millot, C.: Variability of the northern current off Marseilles, western Mediterranean Sea, from February to June 1992, Oceanol. Acta, 18, 193–205, https://doi.org/10.1016/0399-1784(95)00009-Q, 1995.

Copin-Montégut, C.: Alkalinity and carbon budgets in the Mediterranean Sea, Global Biogeochem. Cycles, 7, 915–925, https://doi.org/10.1029/93GB01740, 1993.

Copin-Montégut, C., and Bégovic, M.: Distributions of carbonate properties and oxygen along the water column (0–2000 m) in the central part of the NW Mediterranean Sea (Dyfamed site): Influence of winter vertical mixing on air–sea CO2 and O2 exchanges, Deep Sea Res. Part II Top. Stud. Oceanogr., 49, 2049–2066, https://doi.org/10.1016/S0967-0645(02)00027-9, 2002.

Copin-Montégut, C., Bégovic, M., and Merlivat, L.: Variability of the partial pressure of CO2 on diel to annual time scales in the Northwestern Mediterranean Sea, Mar. Chem., 85, 169–189, https://doi.org/10.1016/j.marchem.2003.10.005, 2004.

Coppola, L., Boutin, J., Gattuso, J. P., Lefevre, D., and Metzl, N.: The Carbonate System in the Ligurian Sea, in: Mediterr. Sea Era Glob. Chang. 1 30 Years Multidiscip. Study Ligurian Sea, 79–103, https://doi.org/10.1002/9781119706960.CH4, 2020.

Cossarini, G., Feudale, L., Teruzzi, A., Bolzon, G., Coidessa, G., Solidoro, C., ... and Salon, S.: High-resolution reanalysis of the Mediterranean Sea biogeochemistry (1999–2019), Front. Mar. Sci., 8, 741486, https://doi.org/10.3389/fmars.2021.741486, 2021.

Curbelo-Hernández, D., González-Dávila, M., González, A. G., González-Santana, D., and Santana-Casiano, J. M.: CO2 fluxes in the Northeast Atlantic Ocean based on measurements from a surface ocean observation platform, Sci. Total Environ., 775, 145804, https://doi.org/10.1016/j.scitotenv.2021.145804, 2021a.

Curbelo-Hernández, D., González-Dávila, M., and Santana-Casiano, J. M.: The carbonate system and air-sea CO2 fluxes in coastal and open-ocean waters of the Macaronesia, Front. Mar. Sci., 10:1094250. https://doi.org/10.3389/fmars.2023.1094250, 2023.

© Author(s) 2024. CC BY 4.0 License.

Curbelo-Hernández, D., Pérez, F. F., González-Dávila, M., Gladyshev, S. V., González, A. G., González-Santana, D., Velo, A., Sokov, A., and Santana-Casiano, J. M.: Ocean Acidification trends and Carbonate System dynamics in the North Atlantic Subpolar Gyre during 2009–2019, EGUsphere [preprint], https://doi.org/10.5194/egusphere-2024-1388, 2024.

Curbelo-Hernández, D., Santana-Casiano, J. M., González, A. G., and González-Dávila, M.: Air-Sea CO2 Exchange in the Strait of Gibraltar, Front. Mar. Sci., 8, 1701, https://doi.org/10.3389/FMARS.2021.745304, 2021b.

De Carlo, E. H., Mousseau, L., Passafiume, O., and Drupp, P. S., and Gattuso, J. P.: Carbonate Chemistry and Air-Sea CO2 Flux in a NW Mediterranean Bay Over a Four-Year Period: 2007-2011, Aquat. Geochemistry, 19, 399–442, https://doi.org/10.1007/s10498-013-9217-4, 2013.

de la Paz, M., Gómez-Parra, A., and Forja, J.: Seasonal variability of surface fCO2 in the Strait of Gibraltar, Aquat. Sci., 71, 55–64, https://doi.org/10.1007/s00027-008-8060-y, 2009.

de la Paz, M., Huertas, E. M., Padín, X. A., González-Dávila, M., Santana-Casiano, J. M., Forja, J. M., Orbi, A., Pérez, F. F., and Ríos, A. F.: Reconstruction of the seasonal cycle of air-sea CO2 fluxes in the Strait of Gibraltar, Mar. Chem., 126, 155–162, https://doi.org/10.1016/j.marchem.2011.05.004, 2011.

Dickson, A. G.: Standard potential of the reaction: AgCl(s) + 1/2H2(g) = Ag(s) + HCl(aq), and the standard acidity constant of the ion HSO4- in synthetic sea water from 273.15 to 318.15 K, J. Chem. Thermodyn., 22, 113–127, https://doi.org/10.1016/0021-9614(90)90074-Z, 1990.

Dickson, A. G., and Goyet, C.: Handbook of methods for the analysis of the various parameters of the carbon dioxide system in sea water, Version 2, https://doi.org/10.2172/10107773, 1994.

Dickson, A. G., Sabine, C. L., and Chistian, J. R.: Guide to best practices for ocean CO2 measurements, PICES Special Publ. 3:191, 2007.

https://doi.org/10.5194/egusphere-2024-2709
Preprint. Discussion started: 7 October 2024
© Author(s) 2024. CC BY 4.0 License.

Dohan, K.: Journal of Geophysical Research: Oceans, J. Geophys. Res. Ocean., 122, 2647–2651, https://doi.org/10.1002/2016JC012144, 2017.

Doney, S. C., Fabry, V. J., Feely, R. A., and Kleypas, J. A.: Ocean Acidification: The Other CO2 Problem, Ann. Rev. Mar. Sci., 1, 169–192, https://doi.org/10.1146/annurev.marine.010908.163834, 2009.

D'Ortenzio, F., Antoine, D., and Marullo, S.: Satellite-driven modeling of the upper ocean mixed layer and air-sea CO2 flux in the Mediterranean Sea, Deep Sea Res. Part I Oceanogr. Res. Pap., 55, 405–434, https://doi.org/10.1016/j.dsr.2007.12.008, 2008.

Echevarría, F., García Lafuente, J., Bruno, M., Gorsky, G., Goutx, M., González, N., García, C. M., Gómez, F., Vargas, J. M., Picheral, M., Striby, L., Varela, M., Alonso, J. J., Reul, A., Cózar, A., Prieto, L., Sarhan, T., Plaza, F., and Jiménez-Gómez, F.: Physical-biological coupling in the Strait of Gibraltar, Deep Sea Res. Part II Top. Stud. Oceanogr., 49, 4115–4130, https://doi.org/10.1016/S0967-0645(02)00145-5, 2002.

Escudier, R., Clementi, E., Omar, M., Cipollone, A., Pistoia, J., Aydogdu, A., Drudi, M., Grandi, A., Lyubartsev, V., Lecci, R., Cretí, S., Masina, S., Coppini, G., and Pinardi, N.: Mediterranean Sea Physical Reanalysis (CMEMS MED-Currents) (Version 1) [Data set], Copernicus Monitoring Environment Marine Service (CMEMS), https://doi.org/10.25423/CMCC/MEDSEA_MULTIYEAR_PHY_006_004_E3R1, 2020.

Escudier, R., Clementi, E., Cipollone, A., Pistoia, J., Drudi, M., Grandi, A., Lyubartsev, V., Lecci, R., Aydogdu, A., Delrosso, D., Omar, M., Masina, S., Coppini, G., and Pinardi, N.: A High Resolution Reanalysis for the Mediterranean Sea, Front. Earth Sci., 9, 1060, https://doi.org/10.3389/feart.2021.702285, 2021.

Fassbender, A. J., Schlunegger, S., Rodgers, K. B., and Dunne, J. P.: Quantifying the Role of Seasonality in the Marine Carbon Cycle Feedback: An ESM2M Case Study, Global Biogeochem. Cycles, 36, 1–15, https://doi.org/10.1029/2021GB007018, 2022.

Folkard, A. M., Davies, P. A., Fiúza, A. F. G., and Ambar, I.: Remotely sensed sea surface thermal patterns in the Gulf of Cadiz and the Strait of Gibraltar: Variability, correlations,

https://doi.org/10.5194/egusphere-2024-2709
Preprint. Discussion started: 7 October 2024
© Author(s) 2024. CC BY 4.0 License.

and relationships with the surface wind field, J. Geophys. Res. Ocean., 102, 5669–5683, https://doi.org/10.1029/96JC02505, 1997.

Ford, D. J., Tilstone, G. H., Shutler, J. D., and Kitidis, V.: Identifying the biological control of the annual and multi-year variations in South Atlantic air-sea CO2 flux, Biogeosciences, 19, 4287–4304, https://doi.org/10.5194/bg-19-4287-2022, 2022.

Frankignoulle, M., and Borges, A. V.: European continental shelf as a significant sink for atmospheric carbon dioxide, Global Biogeochem. Cycles, 15, 569–576, https://doi.org/10.1029/2000GB001307, 2001.

Friedlingstein, P., O'Sullivan, M., Jones, M. W., Andrew, R. M., Bakker, D. C. E., Hauck, J., Landschützer, P., Le Quéré, C., Luijkx, I. T., Peters, G. P., Peters, W., Pongratz, J., Schwingshackl, C., Sitch, S., Canadell, J. G., Ciais, P., Jackson, R. B., Alin, S. R., Anthoni, P., Barbero, L., Bates, N. R., Becker, M., Bellouin, N., Decharme, B., Bopp, L., Brasika, I. B. M., Cadule, P., Chamberlain, M. A., Chandra, N., Chau, T.-T.-T., Chevallier, F., Chini, L. P., Cronin, M., Dou, X., Enyo, K., Evans, W., Falk, S., Feely, R. A., Feng, L., Ford, D. J., Gasser, T., Ghattas, J., Gkritzalis, T., Grassi, G., Gregor, L., Gruber, N., Gürses, Ö., Harris, I., Hefner, M., Heinke, J., Houghton, R. A., Hurtt, G. C., Iida, Y., Ilyina, T., Jacobson, A. R., Jain, A., Jarníková, T., Jersild, A., Jiang, F., Jin, Z., Joos, F., Kato, E., Keeling, R. F., Kennedy, D., Klein Goldewijk, K., Knauer, J., Korsbakken, J. I., Körtzinger, A., Lan, X., Lefèvre, N., Li, H., Liu, J., Liu, Z., Ma, L., Marland, G., Mayot, N., McGuire, P. C., McKinley, G. A., Meyer, G., Morgan, E. J., Munro, D. R., Nakaoka, S.-I., Niwa, Y., O'Brien, K. M., Olsen, A., Omar, A. M., Ono, T., Paulsen, M., Pierrot, D., Pocock, K., Poulter, B., Powis, C. M., Rehder, G., Resplandy, L., Robertson, E., Rödenbeck, C., Rosan, T. M., Schwinger, J., Séférian, R., Smallman, T. L., Smith, S. M., Sospedra-Alfonso, R., Sun, Q., Sutton, A. J., Sweeney, C., Takao, S., Tans, P. P., Tian, H., Tilbrook, B., Tsujino, H., Tubiello, F., van der Werf, G. R., van Ooijen, E., Wanninkhof, R., Watanabe, M., Wimart-Rousseau, C., Yang, D., Yang, X., Yuan, W., Yue, X., Zaehle, S., Zeng, J., and Zheng, B.: Global Carbon Budget 2023, Earth Syst. Sci. Data, 15, 5301–5369, https://doi.org/10.5194/essd-15-5301-2023, 2023.

Fröb, F., Olsen, A., Becker, M., Chafik, L., Johannessen, T., Reverdin, G., and Omar, A.: Wintertime fCO2 Variability in the Subpolar North Atlantic Since 2004, Geophys. Res. Lett., 46, 1580–1590, https://doi.org/10.1029/2018GL080554, 2019.

https://doi.org/10.5194/egusphere-2024-2709
Preprint. Discussion started: 7 October 2024
© Author(s) 2024. CC BY 4.0 License.

Frölicher, T. L., Fischer, E. M., and Gruber, N.: Marine heatwaves under global warming, Nature, 560, 360–364, https://doi.org/10.1038/s41586-018-0383-9, 2018.

García-Ibáñez, M. I., Zunino, P., Fröb, F., Carracedo, L. I., Ríos, A. F., Mercier, H., Olsen, A., and Pérez, F. F.: Ocean acidification in the subpolar North Atlantic: Rates and mechanisms controlling pH changes, Biogeosciences, 13, 3701–3715, https://doi.org/10.5194/bg-13-3701-2016, 2016.

García Lafuente, J., Álvarez Fanjul, E., Vargas, J. M., and Ratsimandresy, A. W.: Subinertial variability in the flow through the Strait of Gibraltar, J. Geophys. Res. Ocean., 107, 1–9, https://doi.org/10.1029/2001jc001104, 2002.

Gómez-Jakobsen, F. J., Mercado, J. M., Cortés, D., and Yebra, L., Salles, S.: A first description of the summer upwelling off the Bay of Algeciras and its role in the northwestern Alboran Sea, Estuar. Coast. Shelf Sci., 225, 106230, https://doi.org/10.1016/j.ecss.2019.05.012, 2019.

González-Dávila, M., and Santana-Casiano, J. M.: Long-term trends of pH and inorganic carbon in the Eastern North Atlantic: the ESTOC site, Front. Mar. Sci., 10, 1–16, https://doi.org/10.3389/fmars.2023.1236214, 2023.

Hersbach, H., Bell, B., Berrisford, P., Biavati, G., Horányi, A., Muñoz Sabater, J., Nicolas, J., Peubey, C., Radu, R., Rozum, I., Schepers, D., Simmons, A., Soci, C., Dee, D., and Thépaut, J.-N.: ERA5 hourly data on single levels from 1940 to present, Copernicus Climate Change Service (C3S) Climate Data Store (CDS), https://doi.org/10.24381/cds.adbb2d47, 2023.

Hoegh-Guldberg, O., Cai, R., Poloczanska, E. S., Brewer, P. G., Sundby, S., Hilmi, K., Fabry, V. J., and Jung, S.: The Ocean, in: Climate Change 2014: Impacts, Adaptation, and Vulnerability. Part B: Regional Aspects, Contribution of Working Group II to the Fifth Assessment Report of the Intergovernmental Panel on Climate Change, edited by: V. R. Barros, C. B. Field, D. J. Dokken, M. D. Mastrandrea, K. J. Mach, T. E. Bilir, M. Chatterjee, K. L. Ebi, Y. O. Estrada, R. C. Genova, B. Girma, E. S. Kissel, A. N. Levy, S. MacCracken, P. R. Mastrandrea, and L. L. White, Cambridge Univ. Press, Cambridge, UK and New York, NY, USA, 1655–1731, 2014.

https://doi.org/10.5194/egusphere-2024-2709
Preprint. Discussion started: 7 October 2024
© Author(s) 2024. CC BY 4.0 License.

Hoegh-Guldberg, O., Jacob, D., Taylor, M., Bindi, M., Brown, S., Camilloni, I., Diedhiou, A., Djalante, R., Ebi, K. L., Engelbrecht, F., Guiot, J., Hijioka, Y., Mehrotra, S., Payne, A., S. I. Seneviratne, A. Thomas, R. Warren, and G. Zhou: Impacts of 1.5ºC Global Warming on Natural and Human Systems, in: Global Warming of 1.5°C: An IPCC Special Report on the Impacts of Global Warming of 1.5°C Above Pre-Industrial Levels and Related Global Greenhouse Gas Emission Pathways, edited by: V. Masson-Delmotte, P. Zhai, H.-O. Pörtner, D. Roberts, J. Skea, P. R. Shukla, A. Pirani, W. Moufouma-Okia, C. Péan, R. Pidcock, S. Connors, J. B. R. Matthews, Y. Chen, X. Zhou, M. I. Gomis, E. Lonnoy, T. Maycock, M. Tignor, and T. Waterfield, Cambridge Univ. Press, Cambridge, UK and New York, NY, USA, 175–312, https://doi.org/10.1017/9781009157940.005, 2018.

Hood, E. M., and Merlivat, L.: Annual to interannual variations of fCO2 in the northwestern Mediterranean Sea: Results from hourly measurements made by CARIOCA buoys, 1995-1997, J. Mar. Res., 59, 113–131, https://doi.org/10.1357/002224001321237399, 2001.

IPCC: Climate Change 2023: Synthesis Report, Contribution of Working Groups I, II and III to the Sixth Assessment Report of the Intergovernmental Panel on Climate Change, edited by: H. Lee and J. Romero, IPCC, Geneva, Switzerland, 35–115, https://doi.org/10.59327/IPCC/AR6-9789291691647, 2023.

Johnson, K. M., Wills, K. D., Butler, D. B., Johnson, W. K., and Wong, C. S.: Coulometric total carbon dioxide analysis for marine studies: maximizing the performance of an automated gas extraction system and coulometric detector, Mar. Chem., 44, 167–187, https://doi.org/10.1016/0304-4203(93)90201-X, 1993.

Lacombe, H., and Richez, C.: The regime of the strait of Gibraltar, Elsevier Oceanogr. Ser., 34, 13–73, https://doi.org/10.1016/S0422-9894(08)71237-6, 1982.

Lee, K., Kim, T. W., Byrne, R. H., Millero, F. J., Feely, R. A., and Liu, Y. M.: The universal ratio of boron to chlorinity for the North Pacific and North Atlantic oceans, Geochim. Cosmochim. Acta, 74, 1801–1811, https://doi.org/10.1016/j.gca.2009.12.027, 2010.

https://doi.org/10.5194/egusphere-2024-2709
Preprint. Discussion started: 7 October 2024
© Author(s) 2024. CC BY 4.0 License.

Lee, K., Tong, L. T., Millero, F. J., Sabine, C. L., Dickson, A. G., Goyet, C., Park, G. H., Wanninkhof, R., Feely, R. A., and Key, R. M.: Global relationships of total alkalinity with salinity and temperature in surface waters of the world's oceans, Geophys. Res. Lett., 33, 1–5, https://doi.org/10.1029/2006GL027207, 2006.

Lewis, E., and Wallace, D.: Program Developed for CO2 System Calculations ORNL/CDIAC-105, Carbon Dioxide Information Analysis Centre, 1998.

López-García, M.J., Millot, C., Font, J., and García-Ladona, E.: Surface circulation variability in the Balearic Basin, J. Geophys. Res., 99, 3285–3296, https://doi.org/10.1029/93JC02114, 1994.

Lovenduski, N.S., Gruber, N., Doney, S.C., and Lima, I.D.: Enhanced CO2 outgassing in the Southern Ocean from a positive phase of the Southern Annular Mode, Global Biogeochem. Cycles, 21, 1–14, https://doi.org/10.1029/2006GB002900, 2007.

Lueker, T.J., Dickson, A.G., and Keeling, C.D.: Ocean pCO2 calculated from dissolved inorganic carbon, alkalinity, and equations for K1 and K2: Validation based on laboratory measurements of CO2 in gas and seawater at equilibrium, Mar. Chem., 70, 105–119, https://doi.org/10.1016/S0304-4203(00)00022-0, 2000.

Macías, D., Bruno, M., Echevarría, F., Vázquez, A., and García, C.M.: Meteorologically-induced mesoscale variability of the North-western Alboran Sea (southern Spain) and related biological patterns, Estuar. Coast. Shelf Sci., 78, 250–266, https://doi.org/10.1016/j.ecss.2007.12.008, 2008.

Macias, D., Garcia-Gorriz, E., and Stips, A.: The seasonal cycle of the Atlantic Jet dynamics in the Alboran Sea: Direct atmospheric forcing versus Mediterranean thermohaline circulation, Ocean Dyn., 66, 137–151, https://doi.org/10.1007/s10236-015-0914-y, 2016.

Marcellin Yao, K., Marcou, O., Goyet, C., Guglielmi, V., Touratier, F., and Savy, J.P.: Time variability of the north-western Mediterranean Sea pH over 1995–2011, Mar. Environ. Res., 116, 51–60, https://doi.org/10.1016/J.MARENVRES.2016.02.016, 2016.

https://doi.org/10.5194/egusphere-2024-2709
Preprint. Discussion started: 7 October 2024
© Author(s) 2024. CC BY 4.0 License.

Marty, J.C.: The DYFAMED time-series program (French-JGOFS), Deep-Sea Res. Part II Top. Stud. Oceanogr., 49, 1963–1964, https://doi.org/10.1016/S0967-0645(02)00021-8, 2002.

Mémery, L., Lévy, M., Vérant, S., and Merlivat, L.: The relevant time scales in estimating the air-sea CO2 exchange in a mid-latitude region, Deep-Sea Res. Part II Top. Stud. Oceanogr., 49, 2067–2092, https://doi.org/10.1016/S0967-0645(02)00028-0, 2002.

Merlivat, L., Boutin, J., Antoine, D., Beaumont, L., Golbol, M., and Vellucci, V.: Increase of dissolved inorganic carbon and decrease in pH in near-surface waters in the Mediterranean Sea during the past two decades, Biogeosciences, 15, 5653–5662, https://doi.org/10.5194/bg-15-5653-2018, 2018.

Millero, F.J., Zhang, J., Lee, K., and Campbell, D.M.: Titration alkalinity of seawater, Mar. Chem., 44, 153–165, https://doi.org/10.1016/0304-4203(93)90009-R, 1993.

Millero, F. J., Morse, J., and Chen, C. T.: The carbonate system in the western Mediterranean Sea, Deep-Sea Res. Part A Oceanogr. Res. Pap., 26, 1395–1404, https://doi.org/10.1016/0198-0149(79)90064-2, 1979.

Millot, C.: Circulation in the Western Mediterranean Sea, J. Mar. Syst., 20, 423–442, https://doi.org/10.1016/S0924-7963(98)00078-5, 1999.

Millot, C., and Taupier-Letage, I.: Circulation in the Mediterranean Sea, in: The Mediterranean Sea, edited by: S. G. The Mediterranean Sea, 29–66, 2005.

Minas, H.J., Coste, B., Le Corre, P., Minas, M., and Raimbault, P.: Biological and geochemical signatures associated with the water circulation through the Strait of Gibraltar and in the western Alboran Sea, J. Geophys. Res., 96, 8755–8771, https://doi.org/10.1029/91JC00360, 1991.

Mintrop, L., Pérez, F.F., González-Dávila, M., Santana-Casiano, J.M., and Körtzinger, A.: Alkalinity determination by potentiometry: Intercalibration using three different methods, Ciencias Mar., 26, 23–37, https://doi.org/10.7773/cm.v26i1.573, 2000.

Nielsen, J. N.: Hydrography of the Mediterranean and adjacent seas, Danish Oceanogr. Exped., 1908–10, Report I, 72–191, 1912.

https://doi.org/10.5194/egusphere-2024-2709
Preprint. Discussion started: 7 October 2024
© Author(s) 2024. CC BY 4.0 License.

Nigam, T., Escudier, R., Pistoia, J., Aydogdu, A., Omar, M., Clementi, E., Cipollone, A., Drudi, M., Grandi, A., Mariani, A., Lyubartsev, V., Lecci, R., Cretí, S., Masina, S., Coppini, G., and Pinardi, N.: Mediterranean Sea Physical Reanalysis INTERIM (CMEMS MED-Currents, E3R1i system) (Version 1) [Data set], Copernicus Monitoring Environment Marine Service (CMEMS), https://doi.org/10.25423/CMCC/MEDSEA_MULTIYEAR_PHY_006_004_E3R1I, 2021.

Oliver, E.C.J., Donat, M.G., Burrows, M.T., Moore, P.J., Smale, D.A., Alexander, L.V., Benthuysen, J.A., Feng, M., Sen Gupta, A., Hobday, A.J., Holbrook, N.J., Perkins-Kirkpatrick, S.E., Scannell, H.A., Straub, S.C., and Wernberg, T.: Longer and more frequent marine heatwaves over the past century, Nat. Commun., 9, 1–12, https://doi.org/10.1038/s41467-018-03732-9, 2018.

Orr, J. C., Epitalon, J.-M., Dickson, A. G., and Gattuso, J.-P.: Routine uncertainty propagation for the marine carbon dioxide system, Mar. Chem., 207, 84–107, https://doi.org/10.1016/j.marchem.2018.10.006, 2018.

Padin, X.A., Vazquez-Rodriguez, M., Castaño, M., Velo, A., Alonso-Perez, F., Gago, J., Gilcoto, M., Alvarez, M., Pardo, P.C., De La Paz, M., Rios, A.F., and Pérez, F.F.: Air-Sea CO2 fluxes in the Atlantic as measured during boreal spring and autumn, Biogeosciences, 7, 1587–1606, https://doi.org/10.5194/bg-7-1587-2010, 2010.

Palmiéri, J., Orr, J.C., Dutay, J.-C., Béranger, K., Schneider, A., Beuvier, J., and Somot, S.: Simulated anthropogenic CO2 storage and acidification of the Mediterranean Sea, Biogeosciences, 12, 781–802, https://doi.org/10.5194/bg-12-781-2015, 2015a.

Palmiéri, J., Orr, J.C., Dutay, J.C., Béranger, K., Schneider, A., Beuvier, J., and Somot, S.: Simulated anthropogenic CO2 storage and acidification of the Mediterranean Sea, Biogeosciences, 12, 781–802, https://doi.org/10.5194/bg-12-781-2015, 2015b.

Peliz, A., Boutov, D., and Teles-Machado, A.: The Alboran Sea mesoscale in a long term high resolution simulation: Statistical analysis, Ocean Model., 72, 32–52, https://doi.org/10.1016/j.ocemod.2013.07.002, 2013.

https://doi.org/10.5194/egusphere-2024-2709
Preprint. Discussion started: 7 October 2024
© Author(s) 2024. CC BY 4.0 License.

Peliz, Á., Teles-Machado, A., Marchesiello, P., Dubert, J., and Lafuente, J.G.: Filament generation off the Strait of Gibraltar in response to gap winds, Dyn. Atmos. Ocean., 46, 36–45, https://doi.org/10.1016/j.dynatmoce.2008.08.002, 2009.

Pérez, F.F., and Fraga, F.: Association constant of fluoride and hydrogen ions in seawater, Mar. Chem., 21, 161–168, https://doi.org/10.1016/0304-4203(87)90036-3, 1987.

Pérez, F.F., Olafsson, J., Ólafsdóttir, S.R., Fontela, M., and Takahashi, T.: Contrasting drivers and trends of ocean acidification in the subarctic Atlantic, Sci. Rep., 11, 1–16, https://doi.org/10.1038/s41598-021-93324-3, 2021.

Pierrot, D., Neill, C., Sullivan, K., Castle, R., Wanninkhof, R., Lüger, H., Johannessen, T., Olsen, A., Feely, R.A., and Cosca, C.E.: Recommendations for autonomous underway pCO2 measuring systems and data-reduction routines, Deep-Sea Res. Part II Top. Stud. Oceanogr., 56, 512–522, https://doi.org/10.1016/j.dsr2.2008.05.014, 2009.

Pinot, J. M., Tintoré, J., and Gomis, D.: Multivariate analysis of the surface circulation in the Balearic Sea, Prog. Oceanogr., 36, 343–376, https://doi.org/10.1016/0079-6611(96)00003-1, 1995.

Rayner, N. A., Parker, D. E., Horton, E. B., Folland, C. K., Alexander, L. V., Rowell, D. P., Kent, E. C., and Kaplan, A.: Global analyses of sea surface temperature, sea ice, and night marine air temperature since the late nineteenth century, J. Geophys. Res. Atmos., 108, https://doi.org/10.1029/2002jd002670, 2003.

Renault, L., Oguz, T., Pascual, A., Vizoso, G., and Tintore, J.: Surface circulation in the Alboran Sea (western Mediterranean) inferred from remotely sensed data, J. Geophys. Res. Ocean., 117, 1–11, https://doi.org/10.1029/2011JC007659, 2012.

Richez, C., and Kergomard, C.: Characteristic features occurring in the Strait of Gibraltar as seen through remote sensing data, Phys. Oceanogr. sea straits, 441–455, https://doi.org/10.1007/978-94-009-0677-8_21, 1990.

Rivaro, P., Messa, R., Massolo, S., and Frache, R.: Distributions of carbonate properties along the water column in the Mediterranean Sea: Spatial and temporal variations, Mar. Chem., 121, 236–245, https://doi.org/10.1016/j.marchem.2010.01.007, 2010.

https://doi.org/10.5194/egusphere-2024-2709
Preprint. Discussion started: 7 October 2024
© Author(s) 2024. CC BY 4.0 License.

Robinson, A. R., and Golnaraghi, M.: The physical and dynamical oceanography of the Mediterranean Sea, in: Ocean Processes in Climate Dynamics: Global and Mediterranean Examples, edited by: A. R. Robinson and K. Brink, 255–306, Dordrecht: Springer Netherlands, 1994.

Robinson, A. R., Leslie, W. G., Theocharis, A., and Lascaratos, A.: Mediterranean Sea circulation, Ocean Currents, 1, 19, 2001.

Rodgers, K. B., Schwinger, J., Fassbender, A. J., Landschützer, P., Yamaguchi, R., Frenzel, H., Stein, K., Müller, J. D., Goris, N., Sharma, S., Bushinsky, S., Chau, T. T. T., Gehlen, M., Gallego, M. A., Gloege, L., Gregor, L., Gruber, N., Hauck, J., Iida, Y., Ishii, M., Keppler, L., Kim, J. E., Schlunegger, S., Tjiputra, J., Toyama, K., Vaittinada Ayar, P., and Velo, A.: Seasonal Variability of the Surface Ocean Carbon Cycle: A Synthesis, Global Biogeochem. Cycles, 37, 1–34, https://doi.org/10.1029/2023GB007798, 2023.

Sammari, C., Millot, C., and Prieur, L.: Aspects of the seasonal and mesoscale variabilities of the Northern Current in the western Mediterranean Sea inferred from the PROLIG-2 and PROS-6 experiments, Deep-Sea Res. Part I, 42, 893–917, https://doi.org/10.1016/0967-0637(95)00031-Z, 1995.

Sánchez-Garrido, J. C., García Lafuente, J., Álvarez Fanjul, E., Sotillo, M. G., and de los Santos, F. J.: What does cause the collapse of the western Alboran gyre? Results of an operational ocean model, Prog. Oceanogr., 116, 142–153, https://doi.org/10.1016/j.pocean.2013.07.002, 2013.

Sánchez-Garrido, J. C., and Nadal, I.: The Alboran Sea circulation and its biological response: A review, Front. Mar. Sci., 9, 1–15, https://doi.org/10.3389/fmars.2022.933390, 2022.

Sarmiento, J., and Gruber, N.: Ocean Biogeochemical Dynamics, Princeton Univ. Press, Princeton, https://doi.org/10.1515/9781400849079, 2006.

Schneider, A., Tanhua, T., Körtzinger, A., and Wallace, D. W. R.: High anthropogenic carbon content in the eastern Mediterranean, J. Geophys. Res. Ocean., 115, 1–11, https://doi.org/10.1029/2010JC006171, 2010.

https://doi.org/10.5194/egusphere-2024-2709
Preprint. Discussion started: 7 October 2024
© Author(s) 2024. CC BY 4.0 License.

Schroeder, K., García-Lafuente, J., Josey, S. A., Artale, V., Nardelli, B. B., Carrillo, A., ... and Zodiatis, G.: Circulation of the Mediterranean Sea and its variability, in: The Climate of the Mediterranean Region, edited by: M. D. Alpert and L. O. Reinhold, 187, 2012.

Shadwick, E. H., Thomas, H., Comeau, A., Craig, S. E., Hunt, C. W., and Salisbury, J. E.: Air-Sea CO2 fluxes on the Scotian Shelf: Seasonal to multi-annual variability, Biogeosciences, 7, 3851–3867, https://doi.org/10.5194/bg-7-3851-2010, 2010.

Sharp, J. D., Pierrot, D., Humphreys, M. P., Epitalon, J.-M., Orr, J. C., Lewis, E. R., and Wallace, D. W. R.: CO2SYSv3 for MATLAB (Version v3.2.1), Zenodo, https://doi.org/10.5281/zenodo.3950562, 2023.

Sisma-Ventura, G., Bialik, O. M., Yam, R., Herut, B., and Silverman, J.: pCO2 variability in the surface waters of the ultra-oligotrophic Levantine Sea: Exploring the air–sea CO2 fluxes in a fast warming region, Mar. Chem., 196, 13–23, https://doi.org/10.1016/j.marchem.2017.06.006, 2017.

Smale, D. A., Wernberg, T., Oliver, E. C., Thomsen, M., Harvey, B. P., Straub, S. C., ... and Moore, P. J.: Marine heatwaves threaten global biodiversity and the provision of ecosystem services, Nat. Clim. Change, 9, 306–312, https://doi.org/10.1038/s41558-019-0364-4, 2019.

Solé, J., Ballabrera-Poy, J., Macías, D., and Catalán, I. A.: The role of ocean velocity in chlorophyll variability. A modelling study in the Alboran Sea, Sci. Mar., 80, 249–256, https://doi.org/10.3989/scimar.04290.04A, 2016.

Speich, S., Madec, G., and Crépon, M.: A strait outflow circulation process study: The case of the Alboran Sea, J. Phys. Oceanogr., 26, 320–340, https://doi.org/10.1175/1520-0485(1996)026<0320>2.0.CO;2, 1996.

Stanichny, S., Tigny, V., Stanichnaya, R., and Djenidi, S.: Wind driven upwelling along the African coast of the Strait of Gibraltar, Geophys. Res. Lett., 32, 1–4, https://doi.org/10.1029/2004GL021760, 2005.

https://doi.org/10.5194/egusphere-2024-2709
Preprint. Discussion started: 7 October 2024
© Author(s) 2024. CC BY 4.0 License.

Taillandier, V., D'Ortenzio, F., and Antoine, D.: Carbon fluxes in the mixed layer of the Mediterranean Sea in the 1980s and the 2000s, Deep-Sea Res. Part I Oceanogr. Res. Pap., 65, 73–84, https://doi.org/10.1016/j.dsr.2012.03.004, 2012.

Takahashi, T.: Global air-sea flux of CO2 based on surface ocean pCO2, and seasonal biological and temperature effects, Deep-Sea Res. Part II, 49, 1601–1622, 2002.

Takahashi, T., Olafsson, J., Goddard, J. G., Chipman, D. W., and Sutherland, S. C.: Seasonal variation of CO2 and nutrients in the high-latitude surface oceans: A comparative study, Global Biogeochem. Cycles, 7, 843–878, https://doi.org/10.1029/93GB02263, 1993.

Takahashi, T., Sutherland, S. C., Sweeney, C., Poisson, A., Metzl, N., Tilbrook, B., Bates, N., Wanninkhof, R., Feely, R. A., Sabine, C., Olafsson, J., and Nojiri, Y.: Global sea-air CO2 flux based on climatological surface ocean pCO2, and seasonal biological and temperature effects, Deep-Sea Res. Part II Top. Stud. Oceanogr., 49, 1601–1622, https://doi.org/10.1016/S0967-0645(02)00003-6, 2002.

Tanhua, T., Hainbucher, D., Schroeder, K., Cardin, V., Álvarez, M., and Civitarese, G.: The Mediterranean Sea system: A review and an introduction to the special issue, Ocean Sci., 9, 789–803, https://doi.org/10.5194/OS-9-789-2013, 2013.

Touratier, F., and Goyet, C.: Decadal evolution of anthropogenic CO2 in the northwestern Mediterranean Sea from the mid-1990s to the mid-2000s, Deep-Sea Res. Part I Oceanogr. Res. Pap., 56, 1708–1716, https://doi.org/10.1016/J.DSR.2009.05.015, 2009.

Turi, G., Lachkar, Z., and Gruber, N.: Spatiotemporal variability and drivers of pCO2 and air-sea CO2 fluxes in the California Current System: An eddy-resolving modeling study, Biogeosciences, 11, 671–690, https://doi.org/10.5194/BG-11-671-2014, 2014.

Turi, G., Lachkar, Z., Gruber, N., and Münnich, M.: Climatic modulation of recent trends in ocean acidification in the California Current System, Environ. Res. Lett., 11, 014007, https://doi.org/10.1088/1748-9326/11/1/014007, 2016.

Ulses, C., Estournel, C., Marsaleix, P., Soetaert, K., Fourrier, M., Coppola, L., Lefèvre, D., Touratier, F., Goyet, C., Guglielmi, V., Kessouri, F., Testor, P., and Durrieu De

https://doi.org/10.5194/egusphere-2024-2709
Preprint. Discussion started: 7 October 2024
© Author(s) 2024. CC BY 4.0 License.

Madron, X.: Seasonal dynamics and annual budget of dissolved inorganic carbon in the northwestern Mediterranean deep-convection region, Biogeosciences, 20, 4683–4710, https://doi.org/10.5194/bg-20-4683-2023, 2023.

Van Heuven, S., Pierrot, D., Rae, J. W. B., Lewis, E., and Wallace, D. W. R.: MATLAB Program Developed for CO2 System Calculations, ORNL/CDIAC-105b, Carbon Dioxide Information Analysis Center, Oak Ridge National Laboratory, U.S. Department of Energy, Oak Ridge, Tennessee, https://doi.org/10.3334/CDIAC/otg.CO2SYS_MATLAB_v1.1, 2011.

Vargas-Yáez, M., Plaza, F., García-Lafuente, J., Sarhan, T., Vargas, J. M., and Vélez-Belchi, P.: About the seasonal variability of the Alboran Sea circulation, J. Mar. Syst., 35, 229–248, https://doi.org/10.1016/S0924-7963(02)00128-8, 2002.

Viúdez, A., Pinot, J. M., and Haney, R. L.: On the upper layer circulation in the Alboran Sea, J. Geophys. Res. Ocean., 103, 21653–21666, https://doi.org/10.1029/98JC01082, 1998.

Wanninkhof, R.: Relationship between wind speed and gas exchange over the ocean revisited, Limnol. Oceanogr. Methods, 12, 351–362, https://doi.org/10.4319/lom.2014.12.351, 2014.

Wanninkhof, R., Doney, S. C., Peng, T.-H., Bullister, J. L., Lee, K., and Feely, R. A.: Comparison of methods to determine the anthropogenic CO2 invasion into the Atlantic Ocean, Tellus B, 51, 511–530, https://doi.org/10.3402/tellusb.v51i2.16335, 1999.

Wanninkhof, R., Pierrot, D., Sullivan, K., Mears, P., and Barbero, L.: Comparison of discrete and underway CO2 measurements: Inferences on the temperature dependence of the fugacity of CO2 in seawater, Mar. Chem., 247, 104178, https://doi.org/10.1016/j.marchem.2022.104178, 2022.

Whitehead, J. A., and Miller, A. R.: Laboratory simulation of the gyre in the Alboran Sea, J. Geophys. Res. Ocean., 84, 3733–3742, https://doi.org/10.1029/jc084ic07p03733, 1979.

https://doi.org/10.5194/egusphere-2024-2709
Preprint. Discussion started: 7 October 2024
© Author(s) 2024. CC BY 4.0 License.

Wimart-Rousseau, C., Lajaunie-Salla, K., Marrec, P., Wagener, T., Raimbault, P., Lagadec, V., Lafont, M., Garcia, N., Diaz, F., Pinazo, C., Yohia, C., Garcia, F., Xueref-Remy, I., Blanc, P. E., Armengaud, A., and Lefèvre, D.: Temporal variability of the carbonate system and air-sea CO2 exchanges in a Mediterranean human-impacted coastal site, Estuar. Coast. Shelf Sci., 236, https://doi.org/10.1016/j.ecss.2020.106641, 2020.

Wimart-Rousseau, C., Wagener, T., Álvarez, M., Moutin, T., Fourrier, M., Coppola, L., Niclas-Chirurgien, L., Raimbault, P., D'Ortenzio, F., Durrieu de Madron, X., Taillandier, V., Dumas, F., Conan, P., Pujo-Pay, M., and Lefèvre, D.: Seasonal and Interannual Variability of the CO2 System in the Eastern Mediterranean Sea: A Case Study in the North Western Levantine Basin, Front. Mar. Sci., 8, 1–18, https://doi.org/10.3389/fmars.2021.649246, 2021.

Wimart-Rousseau, C., Wagener, T., Bosse, A., Raimbault, P., Coppola, L., Fourrier, M., Ulses, C., and Lefèvre, D.: Assessing seasonal and interannual changes in carbonate chemistry across two time-series sites in the North Western Mediterranean Sea, Front. Mar. Sci., 10, https://doi.org/10.3389/fmars.2023.1281003, 2023.

Zarghamipour, M., Malakooti, H., and Bordbar, M. H.: Air–Sea CO2 Exchange Over the Mediterranean Sea, the Red Sea and the Arabian Sea, Int. J. Environ. Res., 18, https://doi.org/10.1007/s41742-024-00586-6, 2024.